Polymer Reaction Engineering Tools to Tailor Smart and Superabsorbent Hydrogels

17

Catarina P. Gomes, Rolando C. S. Dias, and Mário Rui P. F. N. Costa

Contents

C. P. Gomes · R. C. S. Dias (✉)
LSRE and Centro de Investigação de Montanha (CIMO), Instituto Politécnico de Bragança, Campus de Santa Apolónia, Bragança, Portugal
e-mail: rdias@ipb.pt

M. R. P. F. N. Costa
LSRE-Faculdade de Engenharia da Universidade do Porto, Porto, Portugal

Md. I. H. Mondal (ed.), *Cellulose-Based Superabsorbent Hydrogels*,
Polymers and Polymeric Composites: A Reference Series,
https://doi.org/10.1007/978-3-319-77830-3_19

Abstract

Experimental and theoretical tools to describe and tailor polymer network formation processes are here addressed. Although a special emphasis is given to the synthesis, characterization, and applications of smart and superabsorbent polymers, other networks with higher cross-linker contents are also prospected. Purely synthetic and cellulose-based hydrogels are both considered in this research. The reactor type (e.g., batch or continuous flow micro-reactor), polymerization process (e.g., bulk, inverse suspension, or precipitation polymerization), and polymerization mechanism (e.g., classic free radical polymerization or reversible deactivation radical polymerization RDRP) are highlighted as possible tools to change the morphology and the molecular architecture of polymer networks and hydrogels. The tailoring of cellulose-synthetic hybrid materials is also addressed through the use of RAFT-mediated polymer grafting. Case studies showing the applications of the synthesized materials are presented, namely, molecularly imprinted hydrogel particles for retention of aminopyridines, molecularly imprinted polymers for polyphenols, caffeine or 5-fluorouracil selective uptake/release, as well as modified cellulose adsorbents for polyphenol retention. Cellulose-based hydrogels are also considered as possible vehicles for polyphenol-controlled release. The mechanisms of liberation of polyphenols from these materials are analyzed, namely, when supercritical CO_2 is used in the hydrogel impregnation process.

Keywords

Polymer networks · Hydrogels · Cellulose · Modeling · RAFT polymerization · Molecular imprinting · Controlled release

1 Introduction

Hydrogels are generically defined as low cross-linked hydrophilic polymer networks. Owing to their unique properties, hydrogels present useful applications in medicine and pharmaceutics, hygiene and sanitary industries, agriculture, environment, separation processes, and others [1, 2]. Indeed, due to the swelling capacity of

these kinds of polymer networks, hydrogels are able to absorb a large amount of water without being themselves dissolved. Moreover, some kinds of hydrogels present responsive swelling or shrinking triggered by changes in parameters such as temperature, pH, electric/magnetic fields, ionic strength, etc. These materials, often called "stimuli-responsive" or "smart" hydrogels, exhibit reversible transitions between shrunk and swollen states that are macroscopically apparent. Neutralization of charged groups present in the polymer network due to pH shift and changes in hydrogen-bonding efficiency or in ionic strength are examples of mechanisms inducing such reversible transitions in hydrogels [1].

Polymer networks with the specific ability to absorb huge amounts of water relatively to their dry weight are often called superabsorbent polymers (SAPs). Superabsorbent behavior of such kinds of materials is driven by the water dissolution into the polymer network when it is enhanced by the presence of dissociated ionic pendant functional groups due to a strong solvation process. The difference between a traditional absorbent material (e.g., a polyurethane sponge) and a SAP becomes evident when their absorbencies (mass of absorbed water per mass of dry material) are compared: 10 g/g for polyurethane sponge and up to 1000 g/g for acrylic SAP [2]. It is possible to find polymer gels showing super absorbency features both based on synthetic and natural polymers. Well-known examples of these latter, which generate useful superabsorbent materials, are polysaccharides (such as cellulose), alginates (anionic), chitosan (cationic), and polypeptides (involving physical gelation). On the other hand, polymer networks based upon poly(acrylic acid), polyacrylamide, poly(ethylene oxide), or poly(vinyl alcohol) are commonly used to produce synthetic SAPs. Partially neutralized poly(acrylic acid) networks are especially relevant in SAP industry and present outstanding superabsorbency properties. Hybrid materials containing natural and synthetic polymers, such as starch/polyacrylonitrile or cellulose/poly(acrylic acid), can also be used as superabsorbent materials [2].

Polymers are known to be an important example of "products-by-process" which means that the structure and final properties of the products are mainly defined during the synthesis process [3]. Thus, the molecular architecture of polymer networks, such as smart hydrogels and SAPs, and their end-use properties (e.g., swelling, water absorbency, degree of stimulation, adsorption capabilities, elastic properties) are strongly dependent on the synthesis conditions used in their production. Initial composition, polymerization mechanism (e.g., conventional free radical polymerization or controlled radical polymerization), temperature, and reaction process (e.g., reactor type, solution/bulk/suspension/emulsion polymerization) are examples of key parameters with a crucial effect on the final properties of hydrogels and SAPs. A good knowledge of the mechanisms intervenient in the formation of these kinds of networks is therefore critical in order to make possible a consistent production of advanced materials with tailored properties. Polymer reaction engineering aims at providing the connection between the fundamental kinetic mechanisms occurring during a synthesis process and the microstructure of the resulting polymer and will be here explored in the framework of the production of hydrogel and SAPs. Besides the purely synthetic approach, polymer reaction engineering will be also considered to aid in the production of materials based on synthetic and natural polymers, especially cellulose.

2 Experimental Techniques

2.1 Materials

The following materials were used in the synthesis, purification, and testing of the different kinds of polymers and polymer networks addressed in this research.

Monomers acrylic acid (AA); methacrylic acid (MAA); N-isopropylacrylamide (NIPA); N,N-dimethylacrylamide (DMA); acrylamide (Am); 2-hydroxyethyl methacrylate (HEMA); 2-(dimethylamino)ethyl methacrylate (DMAEMA); and styrene (S) were purchased from Sigma-Aldrich, whereas 4-vinylpyridine (4VP) was provided by Alfa Aesar.

Cross-linkers methylene bisacrylamide (MBAm), trimethylolpropane triacrylate (TMPTA), and ethylene glycol dimethacrylate (EGDMA) were also purchased from Sigma-Aldrich. Polymerization initiators and catalysts 2,2′-azobis(2-methylpropionamidine) dihydrochloride (V50), azobisisobutyronitrile (AIBN), ammonium persulfate (APS), and tetramethylethylenediamine (TEMED) were supplied by Sigma-Aldrich, and 2,2′-azobis[2-(2-imidazolin-2-yl)propane] dihydrochloride (VA-044) was purchased from Wako Chemicals.

RAFT polymerization agents 2-cyano-2-propyl benzodithioate (CYDB), 4-cyano-4-(phenylcarbonothioylthio)pentanoic acid (CPA) and 2-cyano-2-propyl dodecyl trithiocarbonate (CPDT) were purchased from Strem Chemicals. The Sigma-Aldrich commercially available RAFT agents CPA, cyanomethyl dodecyl trithiocarbonate (CDT), S-(thiobenzoyl)thioglycolic acid (TBTGA), and 2-(dodecylthiocarbonothioylthio)-2-methylpropionic acid (DDMAT) were also used in our synthesis tasks. Thioglycolic acid (TA) (Sigma-Aldrich) was used as a chain transfer agent.

Analytical reagent grade acetonitrile (ACN), dimethylformamide (DMF), acetic acid (AcOH), methanol (MeOH), tetrahydrofuran (THF), and acetone were bought from Fisher Chemical (UK). Paraffin oil was received from Vencilab (Portugal). Cyclohexane, n-heptane, dichloromethane, and chloroform were purchased from Sigma-Aldrich. Surfactant sorbitan monooleate (span 80) was purchased from Panreac (Spain). Millipore water (Milli-Q quality) was used in all the experiments unless otherwise mentioned.

Cellulose fibers (medium, cotton linters), microcrystalline cellulose (powder, 20 μm, cotton linters), and Whatman No. 1 cellulose filter paper have been purchased from Sigma-Aldrich and used for the synthesis of cellulose-based hydrogels, the generation of cellulose-based materials with modified physicochemical properties, and also for the production of RAFT-grafted modified cellulose. Sodium hydroxide and urea (Sigma-Aldrich) were used to dissolve cellulose in aqueous solutions. Epichlorohydrin (ECH, Sigma-Aldrich) was used as a cellulose cross-linker. N,N-′-dicyclohexylcarbodiimide (DCC) and 4-(dimethylamino)pyridine (DMAP), both from Sigma-Aldrich, were used as coupling agent and catalyst, respectively, in the Steglich esterification of cellulose with RAFT agents containing carboxylic acid functional groups. Some of the aforementioned monomers were considered in the studies concerning the RAFT-grafting of cellulose, as below discussed in this work.

Different kinds of molecules were considered in retention and release studies involving the polymer networks synthesized as sorbents, namely, 3-aminopyridine (3-APy) and 4-aminopyridine (4-APy) that were obtained from Alfa Aesar. Caffeine (CAF), theophylline (THP), theobromine (THB), ibuprofen (IBU), and isoniazid (INH) were procured from Acros Organics. 5-fluorouracil (5FU), uracil (UR), thymine (THY), and polydatin (POL) were purchased from Sigma-Aldrich.

2.2 Reaction Apparatus and Instruments

Different kinds of reaction apparatus have been used in the synthesis performed in the framework of this research, namely, (i) an atmospheric stirred reactor with maximum capacity of 2.5 L; (ii) a Parr 5100 pressurized glass reactor, mechanically stirred, with 1 L capacity and maximum operation pressure P = 10 bar; and (iii) a supercritical reaction/extraction unit assembled by Paralab SA. This latter unit comprises a Parr 970 mL steel reaction/extraction vessel with mechanical stirring, a pumping system to supply carbon dioxide, control and purge valves, back pressure regulator (BPR), and a trap collector. An automatic control system allows the specification of the set points for the temperature of the coil used to heat the inlet CO_2, temperature of the reactor/extractor, temperature of the BPR, and the temperature of the trap. The amount of CO_2 supplied to the vessel is controlled through a Coriolis flowmeter (mini CORI-FLOW Bronkhorst). The maximum operation temperature and pressure are T = 350 °C and P = 200 bar. (iv) Glass vessels with magnetic stirring were chosen in order to perform batch polymerizations at smaller scales (e.g., 20 mL total volume). (v) A continuous flow micro-reactor including two Knauer HPLC pumps (model Azura P 4. 1S, titanium head) with maximum delivery pressure of 40 MPa and flow rate in the range 0.001 to 10 mL/min is also used in our research. Valco tee devices connect the two lines coming from the pumps with generation of the feed to the micro-reactor. Different tubes with variable internal diameters and lengths (e.g., PTFE tubing with ID ranging from 0.2 to 1.5 mm and L = 20 m) can be used as continuous flow micro-reactors. The micro-reactor tubing is immersed in an oil bath at controlled temperature, and a container at the outlet collects the carrier fluid (e.g., liquid paraffin, cyclohexane) and the polymer particles (e.g., hydrogel particles). A flow of dry argon was used in all the synthesis processes to purge the reactants.

A size exclusion chromatography (SEC) apparatus with refractive index (RI) and multi-angle laser light scattering (MALLS) detection, composed of a Polymer Laboratories PL-GPC-50 integrated SEC system with a differential refractometer with a NIR light source of wavelength 950 ± 30 nm, attached to a Wyatt Technology DAWN8$^+$ HELEOS 658 nm MALLS detector, was used in the characterization of the soluble fraction for the different kinds of polymers synthesized. Information concerning the molecular weight distribution, the average molecular weights, and the *z*-average radius of gyration of the soluble polymer population was thus obtained. Monomer conversion was also estimated through the quantification of the correspondent peaks in the SEC analysis. This SEC system was mostly used to

perform the polymer analysis in organic eluents (e.g., THF and DMF). Through a flow-to-batch conversion kit, the MALLS DAWN8$^+$ HELEOS instrument was also used to perform the *in-line* measurement of the scattered light intensity during hydrogel formation, as below described.

Another SEC apparatus was used for the size fractionation of the soluble polymers considering the direct analysis in aqueous eluents with controlled pH. This system is composed of a Viscotek GPCmax VE 2001 integrated solvent and sample delivery module coupled to a tetra-detector array including refractive index, light scattering, viscosity (IV-DP), and ultraviolet (UV) detection.

An Axiom Analytical Attenuated Total Reflection (ATR) immersion probe, model DRR207, was used to carry out the *in-line* monitoring of the polymerization reactions. A three-arm light guide connected the immersion probe to an ABB Bomem Fourier Transform Infrared (FTIR) spectrophotometer model FTLA2000–104. The spectrophotometer was equipped with an ABB Bomem Mercury-Cadmium Telluride (MCT) detector (model D10B) cooled with liquid nitrogen. The optical system is continuously flushed with argon. This FTIR system was also used to perform the *off-line* analysis of polymer samples.

Other apparatus and techniques used for the polymer network cleaning and characterization include Soxhlet extraction, solid-phase extraction (SPE) in a Visiprep (Supelco, Bellefonte, USA) processing station manifold, and batch and continuous mode adsorption/desorption of selected molecules. In the latter case, networks to be tested were packed in empty GPC columns with bed lengths/internal diameters (mm/mm) ranging from 10/4.6 to 300/4.6, and the uptake/release of the analytes was measured in different solvents. *In-line* and *off-line* measurement of UV absorption was used to quantify these processes. Swelling measurements for the different materials was performed through gravimetric analysis. Standard microscopy (in a Nikon Microscope ECLIPSE 50i) and scanning electronic microscopy (SEM) yielded information concerning the morphology of the different hydrogels and other synthesized polymer networks.

3 Synthetic and Cellulose-Based Hydrogels

A possible division in two main classes of chemically cross-linked hydrogels is based on the provenience of the materials considered in their production: synthetic hydrogels that are obtained through the copolymerization of petrochemical-derived monomers and hydrogels including natural polymers such as polysaccharides or polypeptides. Cellulose-based hydrogels will be here specifically considered in the latter case.

3.1 Overview of Synthesis Routes for Hydrogels

A key tool to design synthetic hydrogels is the selection of the monomers leading to the polymer network. For instance, sensitivity to external stimulation of hydrogels

(a critical feature in many applications) can, in principle, be modulated using different kinds of functional monomers. Indeed, AA and MAA are often used to generate anionic hydrogels with high pH sensitivity, whereas DMAEMA, e.g., is often chosen for obtaining cationic hydrogels with inverse pH stimulation in contrast with the former group. NIPA monomer is often chosen for obtaining hydrogels exhibiting temperature stimulation with a critical transition at around T = 32 °C, which is commonly exploited in biomedical applications. Critical transitions triggered by temperature changes at higher ranges (e.g., around 50 °C) are found with other monomers, namely, with DMA. In certain applications, nontoxic and nonionic hydrogels are sought, and, in this case, HEMA-based polymer networks are good candidates owing to their biocompatibility. When mixed effects are to coexist in the same hydrogel, a polymer network including different functionalities can be used. Amphoteric hydrogels based on AA/DMAEMA and pH/temperature-sensitive AA/NIPA are two examples of such kinds of materials.

Another parameter with a huge impact on synthetic hydrogel properties is the cross-linker content. For instance, commercial superabsorbent polymers (SAPs) are mostly produced through the copolymerization of AA with a very small amount of a cross-linker such as MBAm or TMPTA, e.g. Usually this production process is carried out directly in aqueous phase. Hence, the low water solubility of some cross-linkers is an important issue in this context; organic solvents could also be used, but the process would become less eco-friendly and/or with higher operating costs. Both a very high swelling ratio and a low fraction of soluble polymer must be achieved in SAP synthesis, both implying a mole fraction of cross-linker in the global monomer mixture as low as 0.0025 to 0.5%. The degree of neutralization and initial concentration of AA also plays an important role in SAP performance since polymerizations are often directly performed in alkaline aqueous solutions (e.g., 15 to 40% AA in water with 50 to 70% neutralization using NaOH). Industrially, thermal initiation is preferred, with an operation temperature in the range 40 to 70 °C. The final outcome is a sodium acrylate polymer network. Note that a posttreatment of non-neutralized hydrogels with an alkaline solution is also possible, but a lower efficiency is associated with this alternative.

A higher cross-linker content as compared to the one usually chosen for the soft hydrogels (up to 2%), including the SAPs and other kinds of highly swellable hydrogels, leads to stiffer materials presenting advantageous properties when lower swelling in aqueous media is required. Indeed, in some applications (e.g., biomedical, sensing, etc.) a lower and controlled degree of swelling of the networks is sought, and the cross-linker content used in their synthesis can increase to 5–10%. Moreover, in some other materials such as the molecularly imprinted polymers (MIPs) or other kinds of sorbents, a high geometrical stability of the polymer network must be achieved, and a cross-linker content as high as 80% is practically used.

Changes in the morphology and in the porous structure of polymer network materials (including generic hydrogels and SAPs) can also be used to enhance their performance, namely, the intervenient mass transport mechanisms. Introduction of fillers or porogens in the reaction mixture is usually considered with this goal. Additionally, instead of bulk/solution processes, suspension, inverse suspension, emulsion, precipitation, or dispersion polymerization can be used to produce

hydrogel particles with controlled size and shape. Continuous flow micro-reactors have been chosen in the last few years also aiming at the tailoring of the size and shape of these materials. Figure 1a depicts an image of an acrylic hydrogel powder produced in this research through an inverse suspension process. Figure 1b shows the correspondent water-swollen hydrogel. Note that a fast water absorption process is generally observed with this kind of hydrogels and a huge value for the equilibrium swelling ratio is possible (e.g., SR close to 1000, as described in [4] and references therein).

Owing to the huge abundance of cellulose and its biocompatibility, the development of materials incorporating this natural polymer has been carried out in many recent studies. As far as hydrogels are concerned, several different techniques have been studied in the last few years in order to incorporate cellulose in such materials, as reported in some review papers (see [5, 6] and references therein). Chemically cross-linked cellulose-based hydrogels can be obtained through different synthesis routes, making use of the reaction with the OH groups, namely, through bifunctional molecules such as divinylsulfone, epichlorohydrin, or citric acid. Radical cross-linking processes [5] avoid the toxicity problems associated with some bifunctional cross-linkers and offer some advantages for producing cellulose-based hydrogels.

A major problem to be faced when hydrogels are prepared directly from native cellulose is the very low solubility of this polymer in common solvents due to its extensive hydrogen-bonding interactions. Fortunately, new solvents of cellulose have been lately found such as LiCl/dimethylacetamide (LiCl/DMAc), N-methylmorpholine-N-oxide (NMMO), ionic liquids (ILs), and alkali/urea aqueous mixtures [5]. Hydrogel generation can therefore be easily carried out after cellulose dissolution.

3.2 Case Studies with Acrylic and Cellulose/Epichlorohydrin Hydrogels

In Table 1 are presented some recipes used in our research to generate cellulose-based hydrogels. The alkali/urea method for dissolution of cellulose in aqueous systems was chosen including, as reported in the literature [7–9], cycles of cooling

Fig. 1 (**a**) Dried acrylic hydrogel powder obtained through inverse suspension. (**b**) Water-swollen acrylic hydrogel. (**c**) Water-swollen cellulose/epichlorohydrin hydrogel

(e.g., at T = −30 °C) followed by room temperature thawing. Afterward, epichlorohydrin was used as cross-linker, following also the methods before developed [7–9] (24 h reaction time was used in our synthesis). The image of a typical cellulose-based hydrogel obtained under these conditions is presented in Fig. 1c. These results illustrate the possibility for effective cellulose-based hydrogel preparation, using relatively simple processes, following recent research results on this subject [7–9].

The dynamics of swelling and deswelling is a key aspect in the application of hydrogels as superabsorbents, sensors, controlled release vehicles, chromatographic supports, general adsorbents, or biomedical technologies [5]. Obviously, this dynamics and the equilibrium swelling ratio depend on many factors, such as the chemical composition of the hydrogel, the cross-linking density of the network, the morphology and porosity of the materials, etc. Additionally, the swelling conditions, namely, the composition of the solvent, the pH, temperature, and ionic strength, also play a central role on the hydrogel swelling.

Figure 2 illustrates the dynamics of swelling with different kinds of hydrogels synthesized in our research. In Fig. 2a is presented the behavior of an AA-based acrylic hydrogel, obtained in the powdered form through inverse suspension, when dipped either in deionized water or in a 0.9% NaCl aqueous solution. A very fast swelling process is observed, and very high equilibrium swelling ratios are obtained in both conditions, namely, SR~200 in deionized water and SR~100 in 0.9% NaCl aqueous solution. Note however the large drop of swelling ratio when the ionic strength of the solution is increased. Figure 2b shows the dynamics of swelling for two different cellulose-based hydrogels, generated from the cross-linking of microcrystalline and filter paper cellulose with ECH (samples HCEL-5 and HCEL-8 in Table 1). In both cases, the swelling process starts from the dried hydrogels in the form of a single cylinder piece with typical diameter × thickness = 10 × 3 mm × mm. These results put into evidence that the swelling of cellulose-based hydrogels depends strongly on the synthesis conditions used, namely, the kind of cellulose, the dissolution conditions and, among others, the cross-linking conditions. Obviously, changes of the synthesis conditions can be considered to modulate the

Table 1 Synthesis conditions used for cellulose dissolution in aqueous solutions followed by hydrogel preparation with ECH as cross-linker

Hydrogel alias	Cellulose type	NaOH (wt.%)	Urea (wt. %)	CEL (wt. %)	Solution vol. (mL)	ECH vol. (mL)	Preparation T (°C)
HCEL-1	Microcrystalline	7	12	2	10	1	60
HCEL-2	Fibers	7	12	2	10	1	60
HCEL-3	Filter paper	7	12	2	10	1	60
HCEL-4	Fibers	6	4	2	10	1	60
HCEL-5	Microcrystalline	7	12	4	10	1	60
HCEL-6	Fibers	8.6	–	3	6.7	2.14	80
HCEL-7	Microcrystalline	8.6	–	3	6.7	2.14	80
HCEL-8	Filter paper	8.6	–	3	6.7	2.14	80

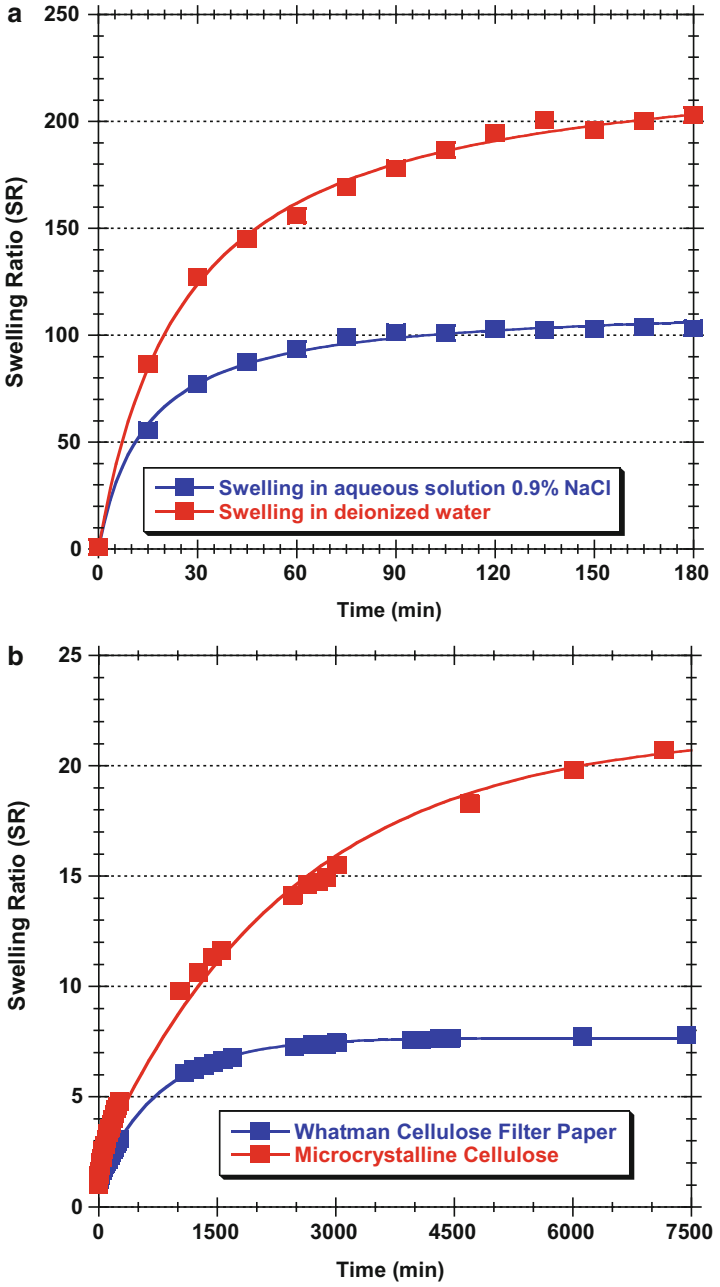

Fig. 2 (**a**) Dynamics of the swelling ratio of an acrylic hydrogel in deionized water and in a 0.9% NaCl aqueous solution. (**b**) Dynamics of the swelling ratio for two different cellulose/epichlorohydrin hydrogels

swelling of the cellulose-based hydrogels in view of the desired application (superabsorbency, controlled release, biomedical, etc.).

The comparison of results presented in Fig. 2a for acrylic hydrogels and in Fig. 2b for cellulose-based hydrogels highlights that considerable differences are observed in the swelling of the two classes of materials. With the selected samples, a much faster swelling dynamics is observed for the acrylic hydrogel comparatively to the cellulose-based networks. Additionally, the equilibrium swelling ratio of the acrylic hydrogels is roughly 10 times higher than that of cellulose materials. Note however that besides the intrinsic chemical differences between the two classes of networks, the morphologies of the products tested are also very distinct (acrylic powder vs. a single piece of cellulose hydrogel). These morphological differences also have a large impact on the dynamics of swelling thus affecting the performance of both kinds of hydrogels. Indeed, several different kinds of parameters are being considered in the scientific community to design these materials. The generation of hybrid hydrogels incorporating both synthetic polymers and cellulose is a promising route in view of the modulation of the properties and the use of sustainable natural resources. The use of synthetic/cellulose interpenetrating polymer networks (IPNs) and grafting of synthetic polymers in cellulose (as below discussed in the present work) are two important approaches to target this issue [5, 6].

The above-presented results illustrate some basic principles involved in the synthesis and application of both synthetic and cellulose-based hydrogels. However, there is plenty of room to improve the structure and properties of these polymer networks concerning the synthetic and the cellulose-based products as well as the hybrid materials. Indeed, a major opportunity to control and design the molecular architecture of polymers was created with the discovery of the reversible deactivation radical polymerization (RDRP) mechanisms. These techniques allow the precise synthesis of many complex structures such as block copolymers, stars, and comb polymers. RDRP mechanisms (e.g., RAFT, ATRP, NMRP) can also be used to achieve improvements of polymer networks, namely, by increasing their structural homogeneity due to the control of the cross-linking process and of the size distribution of the chains between cross-linking points. New grafting processes, functionalization of polymer networks, and creation of complex architectures (e.g., surface brushing) are also possible in the framework of RDRP techniques, especially RAFT polymerization. These new opportunities will be discussed along this work in the context of both the synthetic and the cellulose-based polymer networks.

4 Dynamics of Network Formation and Structural Inhomogeneities

4.1 Light Scattering Measurements and Network Inhomogeneity

The timeline for synthetic network and gel production begins with the vulcanization of natural rubber in the nineteenth century. The synthesis of Bakelite in the beginning of the twentieth century, ion-exchange resins in the 1930s, contact lenses in the

1950s, SAPs and volume phase transition gels in the 1970s, responsive polymers in the 1980s, high strength gels in the beginning of the twenty-first century, and nowadays' synthesis of nearly ideal polymer networks are some important milestones in this context [10]. Different kinds of theories were also developed along the time with the goal of describing the formation, structure, and performance of these materials. Since the 1930s, molecular and phenomenological theories (elasticity, swelling, etc.) were developed by Kuhn, Flory, James, Guth, Treloar, and many others [10]. The entanglement concept in polymer networks was worked out in the 1970s (e.g., Graessley theory), and in a third step, starting in the 1990s until nowadays, the inhomogeneities of polymer networks were addressed using, e.g., Cohen-Colby and Panyukov-Rabin theories [10]. Most of these theories were developed considering the concept of "ideal polymer network" where the sub-chains between cross-links have the same length and defects and entanglements are absent. However, it is known that real polymer networks contain different kinds of irregularities (e.g., distinct kinds of cross-links, through their chemical nature, connectivity, and mobility) due to poor control of the cross-linking process during synthesis, occurrence of side reactions, and inevitable topological complexity of the network structure (such as the presence of short loops). Therefore, the behavior of real polymer networks is far from the expected for a treelike architecture, and an important deleterious effect of the structural inhomogeneities on material performance is often observed.

Thus, the assessment and control of structural inhomogeneities in polymer networks and gels is an important issue that can be addressed considering different approaches. Light scattering studies provide valuable information in this context because an increase in the scattered intensity is commonly observed as a consequence of a cross-linking process. It is accepted that the observed excess scattering is an effect of the polymer structure and shows the degree of heterogeneity of the networks [11]. Often, the practical application of such methods is based upon the evaluation of the difference between the excess scattering of the gel and of the analogous linear polymer solution (formed in the absence of cross-linker), as described in the following equation:

$$R_{ex,q} = R_{gel,q} - R_{sol,q} \tag{1}$$

The Rayleigh ratios for the gel and for the analogous linear polymer solution at the scattering angle θ are obtained through Eq. (2):

$$R_{ex,\theta} = \frac{\left(I_\theta - I_{\theta,solvent}\right) r^2}{I_0 V} \tag{2}$$

Variable I_θ above represents the scattered light intensity at the scattering angle θ, I_0 the intensity of the incident beam, V the volume of the scattering medium, and r the distance between the scattering volume and the detector. Usually, calculations are performed using as independent variable the scattering factor q instead of the scattering angle:

$$q = \frac{4\pi n}{\lambda_0} \sin(\theta/2) \tag{3}$$

With n, λ_0, and θ representing the solvent index of refraction, the wavelength of the incident light, and the scattering angle, respectively.

In practice, it is possible to carry out the *in-line* measurement of the scattered light intensity (I_θ) during the polymer formation [12, 13]. A typical analysis of such kind is presented in Fig. 3 for the polymerization of partially neutralized AA with initiation by APS/TEMED at room temperature. These measurements were performed in a DAWN8+ light scattering instrument and using a flow-to-batch conversion accessory.

From Fig. 3, it can be observed that, after an induction period, the polymerization is accompanied by an increase of the scattered light intensity, eventually reaching a maximum. This maximum corresponds to the critical overlap polymer concentration, and gelation occurs at or slightly beyond this point [12, 13]. Due to the growth of polymer concentration, the scattered light intensity starts to decrease after the critical point. Such kinds of measurements are helpful in the assessment of the spatial heterogeneity of the formed synthetic polymer but can also be used to investigate the formation of gels based on natural polymers, such as cellulose/epichlorohydrin hydrogels (for instance). Additional information concerning the mesh size of the networks and the average molecular weight between cross-linking points ($\bar{M}_c$) can be obtained using dynamic light scattering and mechanical measurements, respectively [12, 13].

4.2 Swelling Analysis

Swelling analysis can also be used to obtain information concerning the average molecular weight between cross-linking points, according the Flory-Rehner theory (see [14, 15] and also Chap. 11 in Ref. [1]):

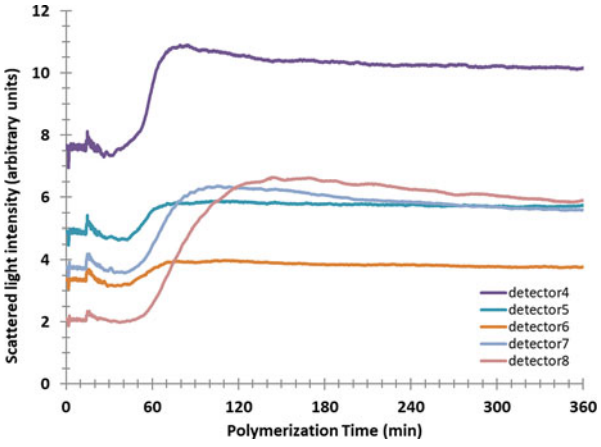

Fig. 3 In-line measurement of the scattered light intensity (I_θ) recorded at different angles (detectors) as a function of the reaction time for the polymerization of partially neutralized AA with initiation by APS/TEMED at room temperature

$$\frac{1}{\bar{M}_c} = \frac{2}{\bar{M}_n} - \frac{\bar{v}\left[\ln(1 - v_N) + v_N + \chi v_N^2\right]}{V_S\left(v_N^{1/3} - v_N/2\right)} \tag{4}$$

In the above equation, V_S stands for the molar volume of the solvent, $\bar{v}$ for the specific volume of the polymer network, v_N for the volume fraction of polymer network in the swollen mass, $\bar{M}_n$ for the molecular weight of the primary polymer chains, and χ for the solvent-polymer interaction parameter (according to Flory-Huggins theory). The volume fraction of polymer network in the swollen mass (v_N) can be experimentally estimated through swelling experiments and is related to the mass swelling ratio by the equation:

$$v_N = \frac{1}{1 + (SR - 1)\dfrac{\rho_N}{\rho_S}} \tag{5}$$

In the above equation ρ_N and ρ_S represent the mass densities of the polymer network and of the solvent, respectively. If the solvent-polymer interaction parameter (χ) is known (estimation methods are also often used [16]), Eq. (4) provides a simple form to measure the $\bar{M}_c$ network parameter. This analysis has been considered in very recent works [17] to assess the homogeneity of polymer networks, namely, through the comparison of gels produced by free radical processes and reversible deactivation radical polymerization (e.g., RAFT polymerization).

4.3 FTIR Analysis of Network Formation

In general, FTIR analysis provides important information concerning polymer formation and final composition of the materials. This technique can also be applied to elucidate the mechanisms of formation of networks and their final chemical functionalities [18–24]. Besides the usual *off-line* analysis of the products [23, 24], *in-line* FTIR monitoring of network development can also be performed [18–22].

In Fig. 4 are presented results concerning the *in-line* FTIR-ATR monitoring of free radical processes involved in typical synthetic hydrogels production, namely, the aqueous polymerization of AA/MBAm (Fig. 4a) and the terpolymerization of MAA/AAm/MBAm (Fig. 4b). These results illustrate the dynamics of change observed in specific peak assignments, showing the polymerization progress.

4.4 Size Exclusion Chromatography

Size exclusion chromatography (SEC) is a powerful technique disclosing important information concerning the soluble polymer species in a specific eluent. In general, for linear polymers, information concerning the entire polymer population is obtained if a proper solvent is available. With nonlinear polymers, although the

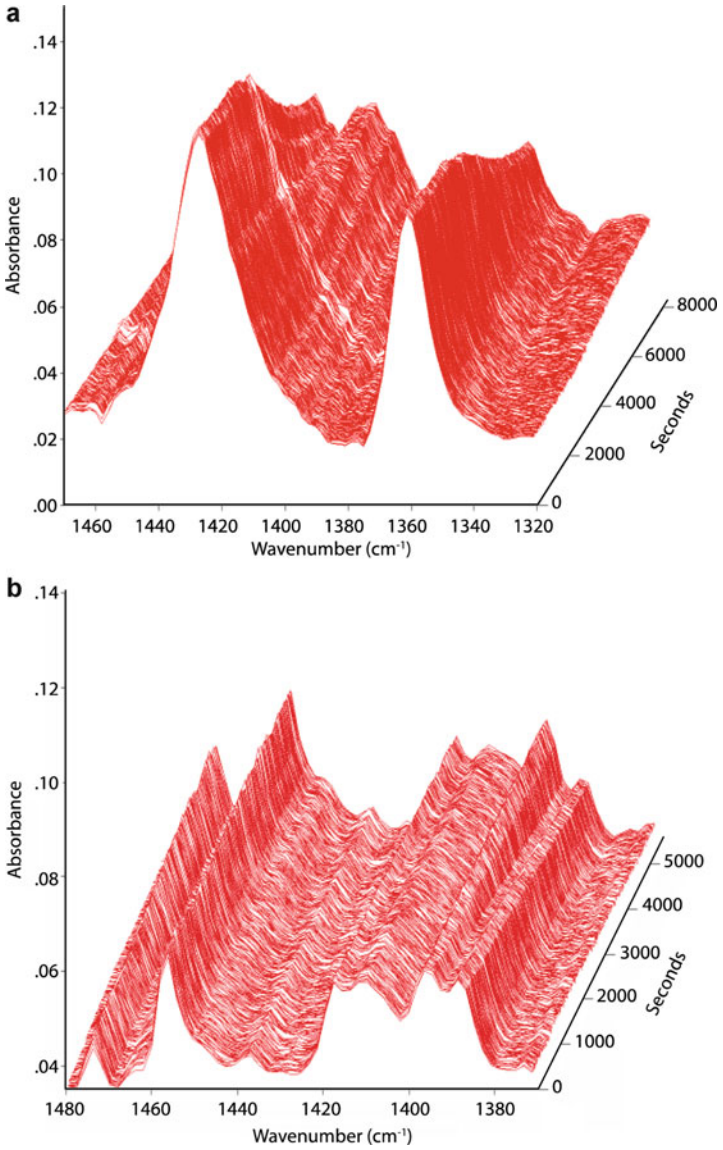

Fig. 4 *In-line* FTIR-ATR monitoring of free radical polymerization processes considered in synthetic hydrogels production: (**a**) aqueous polymerization at room temperature of AA/MBAm (99.5/0.5 mol %), 15% monomer concentration, and 0.1% APS/TEMED. (**b**) Aqueous polymerization at room temperature of MAA/AAm/MBAm initiated by 0.66% APS/TEMED. Initial monomer composition: 13% v/v of MAA in water, 5% w/w of AAm, and 0.5 mol% of MBAm in global monomer composition

soluble phase in the selected solvent can be analyzed by SEC, the superposition of chromatograms of species with different molecular masses or structures but same effective sizes in solution complicates seriously the quantitative analysis. Molecular size distribution and *z*-average radius of gyration are typical structural features that can be investigated through SEC with multiple detection (usually RI and MALLS). Monomer conversion can also be estimated using SEC when the peaks of the involved monomers are detectable in the chromatographic traces.

Some important features provided by SEC analysis in the framework of synthetic hydrogel formation (or their linear counterparts) are presented in Fig. 5. Figure 5a shows the possibility for monomer conversion measurement when the SEC traces of polymer and monomer(s) are identifiable. An inverse suspension RAFT polymerization process, involving the AA and NIPA monomers, is here considered for illustration purposes. Depletion of both monomers in samples collected at different polymerization times is clearly seen. Note that, in the formation of hydrogels, the amount of cross-linker is very small in comparison with the main monomers, and its reliable measurement by SEC is not possible in these conditions.

Figure 5b depicts SEC chromatographic traces for a sample correspondent to the AA/MBAm RAFT polymerization in DMF. The RI and light scattering signals are simultaneously presented in this plot. The existence of soluble polymer is identifiable through the LS and RI signals with the latter also showing the AA monomer peak. Note, however, the huge difference between the RI and LS signals showing the formation of a polymer cluster at a very low concentration (almost nil RI response) but very high molecular size (high LS response). Similar analysis provides useful information concerning the development of the polymer population during the synthesis, namely, an imminent gel formation due to the cross-linking process (predated by the formation of a very large polymer cluster).

In Fig. 5c are compared the LS signals correspondent to samples collected at different polymerization times during inverse suspension DMA RAFT polymerization. The dynamics of the development of a secondary polymer population is here illustrated (see also [21]). Note that these measurements can enlighten key kinetic steps involved in the polymerization mechanisms such as the eventual formation of three-arm adducts during RAFT polymerization due to the termination of intermediate radicals (see [25] and references therein for a detailed discussion on these issues).

Figure 5d compares the SEC analysis correspondent to the FRP of AA in the absence and in the presence of a chain transfer agent (thioglycolic acid was used). The effect of the chain transfer agent on the molecular weight distribution of the polymer is here illustrated, and a possible manipulation of the polymer molecular size through this mechanism is highlighted (a substantial decrease on molecular size is clearly observable). Note that the knowledge on the formation processes and structure of the linear counterparts of the main polymer chains involved in hydrogel formation is critical to understand and tailor the properties of these networks. Indeed, primary chains (those remaining when the cross-links are severed in a network) play a central role in gel formation (as described in Sect. 5) and also in networks properties (elasticity, swelling, and so on). Thus, comparative measurements, such

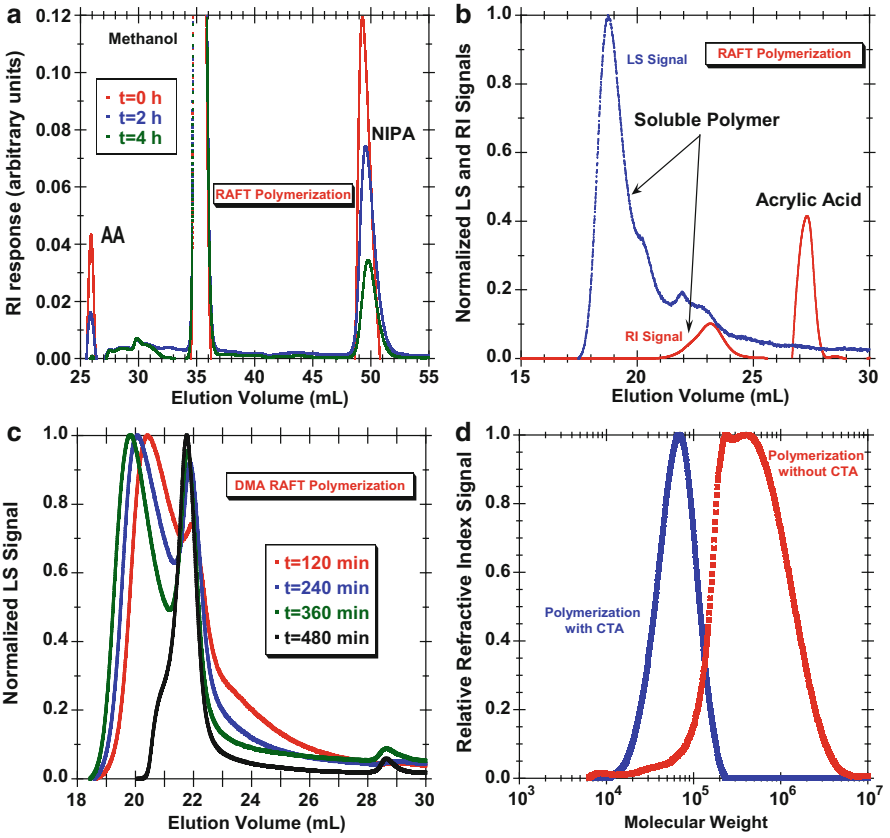

Fig. 5 Results of different SEC analysis carried out for samples of synthetic hydrogels or their linear polymer counterparts. (**a**) Measurement of AA and NIPA concentration in a RAFT copolymerization process involving these two monomers. (**b**) Light scattering and RI signals for an AA-based hydrogel synthesized through RAFT polymerization. (**c**) Light scattering signal for samples correspondent to the DMA RAFT polymerization collected at different polymerization instants. (**d**) Measured effect of the presence of a chain transfer agent (thioglycolic acid) on the molecular weight distribution of an AA polymer

as those provided in Fig. 5a and d for linear polymerization, are helpful to design the hydrogels obtained in similar conditions. In this context, tailoring of the average molecular weight between cross-linking points ($\bar{M}_c$) using RAFT polymerization, as above discussed, is an important opportunity that is being considered in the scientific community.

The knowledge on the kinetics of polymerization plays also an important role on the design and control of hydrogel formation. Some information provided by SEC analysis is illustrated in Fig. 6. The measured dynamics of monomer conversion for AA/MBAm copolymerization with three low contents of MBAm is shown in Fig. 6a. The effect of the degree of neutralization with NaOH in the polymerization

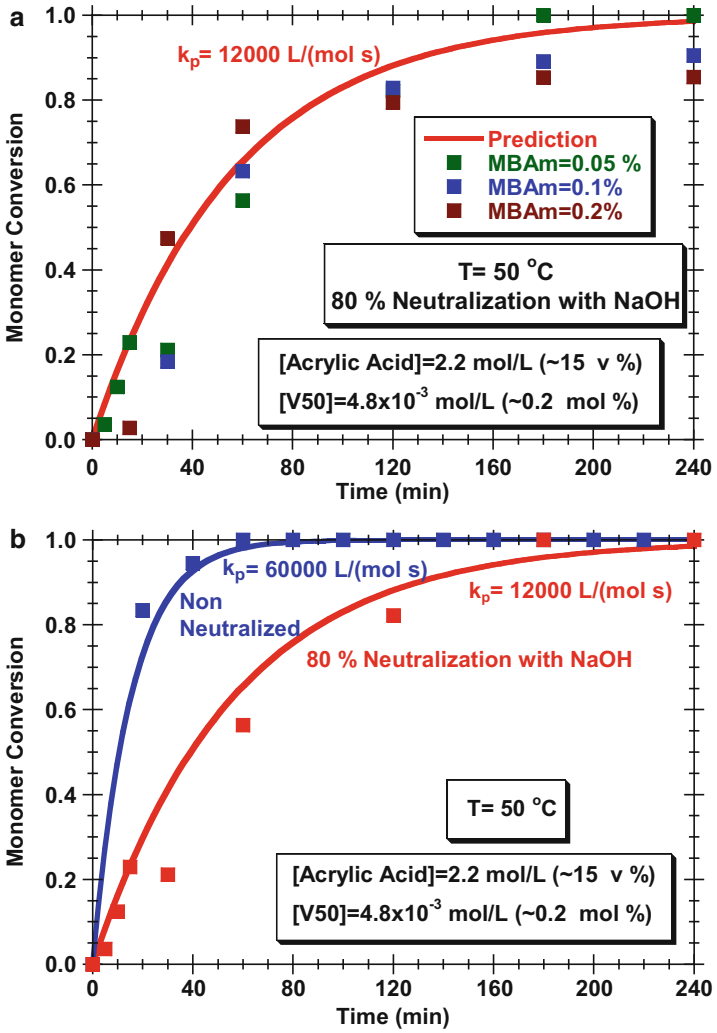

Fig. 6 (**a**) Kinetics of polymerization in an AA/MBAm hydrogel formation obtained by SEC. Cross-linking processes with mole fraction of MBAm ranging from 0.05 to 0.2% were considered. Polymerizations at T = 50 °C with V50 as initiator, concentration of AA ~ 15 v%, and 80% neutralization with NaOH. (**b**) SEC measured effect of the degree of neutralization on the rate of AA polymerization. Non-neutralized and 80% neutralized polymerizations are compared

kinetics is presented in Fig. 6b, evidencing the fall of the polymerization rate when the degree of neutralization is increased. Such kind of experimental data can be used to estimate kinetic parameters (e.g., the propagation rate constants) and to develop models to aid in the design of these polymerization processes, as explored in the next section.

5 Calculation Tools to Describe Network Formation

5.1 Overview

This section presents calculation methods often used to describe the formation of synthetic hydrogels. The modeling of general polymerization process where the branching and cross-linking mechanisms are intervenient is analyzed. The applicability of such tools to design hybrid materials including natural polymers, such as cellulose, is also discussed. Modeling tools for nonlinear RDRP are also briefly addressed.

5.2 Flory-Stockmayer Theory of Gelation

Synthesis of materials presently known to consist of cross-linked synthetic polymers is documented since the first half of the nineteenth century starting with the vulcanization of natural rubber by brothers Charles and Nelson Goodyear.

Along with other important contemporary contributions by W.H. Carothers, W. Kuhn, and G. V. Schulz, it was P.J. Flory [26–30] who laid out the modern foundations of the analysis of polymerization reactions, using either population balances of species [30] or elementary probabilistic deductions [26–29]. The formation of "infinitely" large three-dimensional networks (gels) and the general condition for gelation in condensation polymerization of a symmetrical monomer with f self-reacting groups A_f (such as a silanetriol, with $f = 3$) was established:

$$p_g = \frac{1}{f-1} \tag{6}$$

Here, p is the probability that a chain starting from a branch unit would lead to another branch unit rather than to a terminal group. The derivation of this critical condition is based on a random branching process, as depicted in Fig. 7a for a trifunctional system [26]. Soon afterward, W.H. Stockmayer [31–33] generalized Flory's theory and the whole approach become known as the Flory-Stockmayer (FS) theory of gelation. Using a probabilistic and combinatorial reasoning, W. Stockmayer found in particular an expression for the weight fraction of all isomer species carrying n units for this step-growth polymerization [31]:

$$w(n) = \frac{f(fn-n)!}{(n-1)!(fn-2n+2)!} p^{n-1}(1-p)^{(f-2)n+2} \tag{7}$$

It is worth noting that W. Stockmayer took the trouble to show that Eq. (7) can also be found through the population balance of polymer species, leading him and his contemporaries to believe that both reasonings are always equivalent and lead to the same results, something which would take nearly three decades to be understood as a mistake, as we discuss in the next section. Nevertheless, these results are

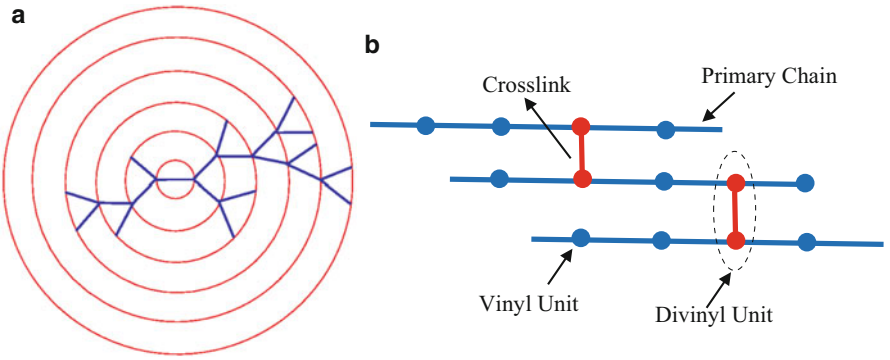

Fig. 7 (**a**) Depiction of the condensation of a trifunctional monomer ($f = 3$) leading to a branched polymer according the Flory's theory: formation of an infinite network is possible if $p > 1/2$ [26]. (**b**) Depiction of the primary chains and cross-links in a network formed through a vinyl/divinyl copolymerization. The same formalism can be used to describe the cross-linking of linear polymer chains (e.g., the cross-linking of cellulose chains)

rigorous for equilibrium step-growth polymerizations and a good approximation even for many chain polymerizations; thence, it is worth pursuing the presentation of these classical findings.

Flory, using the formation of three-dimensional polymers with tetrafunctional branch units as a case study [28], also initiated the extension of the theory of gelation to chain polymerizations. The copolymerization of vinyl and divinyl compounds and the vulcanization of rubber was pointed as two examples involving tetrafunctional branching. Such chemical systems were also later discussed by Stockmayer and co-workers [32, 33], and an expression to predict the critical gelation conversion was derived in the framework of the FS theory:

$$p_g = \frac{1}{y_f\left(\bar{x}_w^* - 1\right)} \tag{8}$$

In Eq. (8), y_f represents the mole fraction of double bonds residing on the divinyl monomer, p_g the conversion of double bonds at the gel point, and $\bar{x}_w^*$ the weight-average chain length of the primary chains. Primary chains are defined as the polymer chains that would remain if every double-reacted divinyl units (cross-links) were severed in the network, as depicted in Fig. 7b (see also the early contribution of Walling for a simplified scheme of vinyl/divinyl copolymerization [34, 35]). Note that the formalism of the FS theory for cross-linking processes can be applied both to the cross-linking of preformed linear polymer chains (e.g., the cross-linking of cellulose that play the role of primary chains) and to the network formation due to vinyl/divinyl copolymerization. In the latter case, the primary chains are considered to be formed during the course of the cross-linking process. Indeed, Flory [28] and Stockmayer [33] derived the expression for the molecular size distribution of the network resulting from the random cross-linking of primary molecules with uniform length:

$$w_P(m) = \frac{m^{m-1}}{\gamma m!}(\gamma e^{-\gamma})^m \tag{9}$$

In Eq. (9), $w_P(m)$ represents the weight fraction of polymer molecules containing m primary chains and γ and the cross-linking index, defined as the number of cross-linked units per primary molecule. On other hand, the cross-linking density of the network (ρ) is defined as the fraction of units that are cross-linked (each cross-linkage bears two cross-linked units, as depicted in Fig. 7b). These two parameters are related through $\gamma = \rho\bar{x}_n^*$, with $\bar{x}_n^*$ representing the number-average chain length of the primary chains.

Note that the critical condition for gelation described by Eq. (8) can be rewritten as $\rho_g\left(\bar{x}_w^* - 1\right) = 1$ with $\rho_g = p_g y_f$ representing the cross-linking density of the network for the vinyl/divinyl system at the gel point (indeed, $p_g y_f$ is the fraction of created cross-linked units at gelation due to the vinyl polymerization process). These equivalences also illustrate the applicability of the FS formalism to the cross-linking of preformed primary chains or the copolymerization of vinyl/divinyl monomers.

For primary polymer chains with uniform length ($\bar{x}_n^* = \bar{x}_w^*$), the critical condition for gelation due to cross-linking is thus $\rho_g\left(\bar{x}_w^* - 1\right) \sim \rho_g\bar{x}_w^* = \rho_g\bar{x}_n^* = 1$, and therefore $\gamma_g = \rho_g\bar{x}_n^* = 1$. For heterogeneous primary chains, the critical cross-linking index is lower than one because $\bar{x}_w^* > \bar{x}_n^*$ (e.g., for primary chains with most probable distribution $\bar{x}_w^* = 2\bar{x}_n^*$, and gelation occurs with cross-linking index $\gamma_g = 1/2$). Note that the theory dealing with the random cross-linking of primary polymer molecules with arbitrary distribution sizes [36] is especially important to describe some processes of gel formation from cellulose chains (e.g., through the cross-linking reactions involving the cellulose hydroxyl groups and epoxides, isocyanates, or carboxylic acids). In particular, it is possible to show that the molecular size distribution for the random cross-linking of a population of primary chains with the most probable distribution is correspondent to the condensation of $A_2 + A_4$ units [36].

FS theory leads to some simple relations valid for the post-gelation period, such as the weight fraction of sol in the random cross-linking of primary chains with uniform length:

$$w_s = e^{-\gamma(1-w_s)} \tag{10}$$

In this equation, w_s represents the weight fraction of sol, while $w_g = 1 - w_s$ stands for the weight fraction of gel. If the size of the primary chains is arbitrarily distributed, the analogue equation for the weight fraction of sol is:

$$w_s = \sum_{n=1}^{\infty} w(n)[1 - \rho(1 - w_s)]^n \tag{11}$$

$w(n)$ in the above equation represents the weight fraction of primary molecules with n units. The applicability of this equation is limited to systems with low cross-linking density ($\rho \ll 1$). Other expressions allow the calculation of the cross-linking density of the sol and the gel as well as the number and weight-average degree of polymerization of the sol before and also after gelation [36]. In Figs. 8, 9, 10, 11, 12, 13,

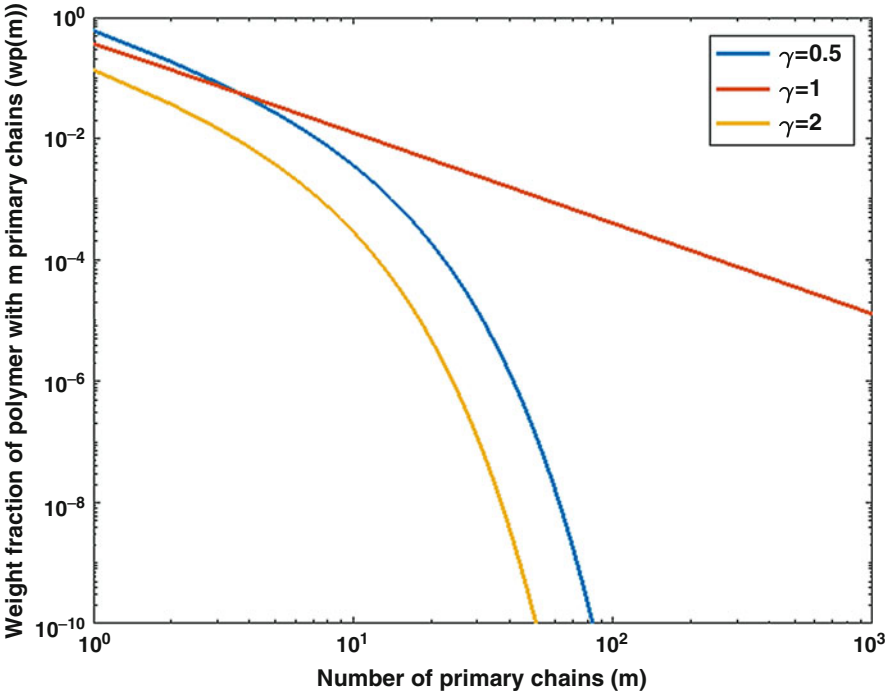

Fig. 8 Weight fraction of polymer with m primary chains, $w_P(m)$, in the random cross-linking of primary molecules with uniform length. Three values for the cross-linking index were selected in order to illustrate the pre-gelation period ($\gamma = 0.5$), gel point ($\gamma = 1$), and the post-gelation ($\gamma = 2$). The overall cross-linking density (ρ) is related with γ through $\gamma = \rho \bar{x}_n^*$ (e.g., with $\bar{x}_n^* = 500$, $\rho = 0.001$, 0.002, and 0.004 for $\gamma = 0.5$, 1, and 2, respectively)

and 14 are illustrated some calculations in the framework of the FS theory, highlighting the possibility to describe relevant variables in cross-linking processes, such as weight fraction of gel, cross-linking density, and molecular weight of the sol and gel.

Note that the above-described calculation methods in the framework of the FS gelation theory can also be applied to the irreversible batch formation of gels such as cellulose-epichlorohydrin polymers. Using a plausible chain length distribution for the primary chains (the cellulose polymer) and taking into account the amount of cross-linker considered in the polymerization (e.g., epichlorohydrin), which defines the number of cross-linkages and therefore the cross-linking density (ρ), the extent of gel formation and the sol/gel properties can be calculated, as above discussed. In practice, the extent of reaction between the OH and epoxy groups and the occurrence of side reactions with epichlorohydrin (e.g., the hydrolysis process in alkaline conditions [7, 8]) are factors with important influence on the real cross-linking density values attained in the gel formation.

The combinatorial reasoning used by Stockmayer is not at all convenient and in 1963 the mathematician I. J. Good and the physical chemist M. Gordon have replaced it with the application of the more powerful *Theory of the Branching*

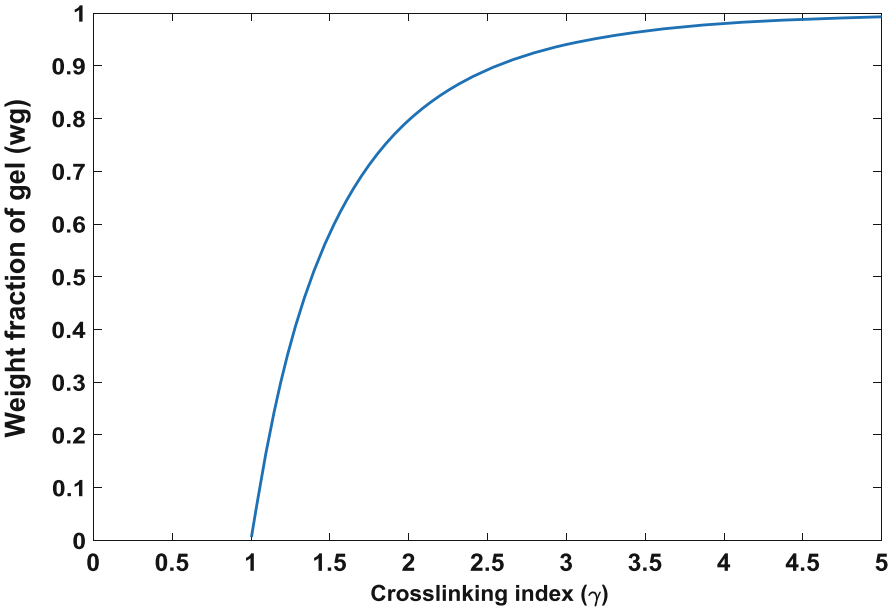

Fig. 9 Weight fraction of gel (w_g) as a function of the cross-linking index (γ) in the random cross-linking of primary molecules with uniform length

Processes (TBP) [37, 38] (with a later impoverished implementation called "recursive approach" by Macosko and Miller [39]). Then, it became possible to tackle chemical systems where different chemical groups and/or substitution effects were present. It then became apparent that some results were not compatible with the analysis by rate equations (see next section).

Another even more important issue is the tackling of intramolecular reactions. Slight disagreements with observed gelation of step-growth polymerizations were long known [27, 28], but the disagreement for chain polymerizations turned out to be very serious [34, 35].

Another issue arises from the stochastic character of real polymerizations leading to fluctuations according to position which diffusion is unable to erase instantaneously. Gelation will not occur for a real network everywhere at the same time even if starting with a perfectly homogeneous mixture. Numerous fundamental studies have used Monte Carlo simulation in a restricted space mesh to gain insight on those phenomena; they have not yet made their way into engineering practice.

5.3 Calculation Methods for Kinetically Controlled Nonrandom Processes

In spite of the appealing simplicity of the FS gelation theory, this approach presents important shortcomings in the description of some cross-linking processes, namely,

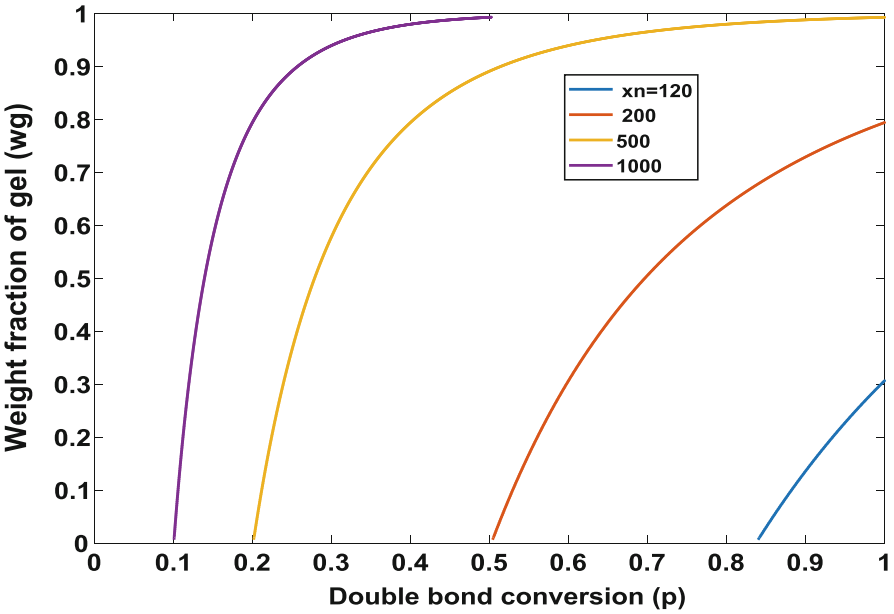

Fig. 10 Weight fraction of gel (w_g) as a function of the double bond conversion (p) in the random cross-linking of vinyl/divinyl monomers. Primary molecules of uniform length but with different values for the number-average chain length ($\bar{x}_n^* = 120$, 200, 500, and 1000) were considered in these simulations. The initial mole fraction of divinyl monomer $y_{DVM} = 0.5\%$ ($y_f \sim 1\%$) is the same in the different systems

when the formation of the primary chains and the network development is simultaneously performed, as in the case of the vinyl/multivinyl copolymerization. Indeed, the free radical copolymerization of multifunctional monomers is a kinetically controlled nonrandom process, and the network properties are critically dependent on the reaction path. It should be stressed that, in a free radical process, polymer molecules present a wide span on birth/death times. Hence, molecules are exposed to very different conditions during the reaction path, and the probability for cross-linking is not homogeneous (e.g., "primary" chains formed at the start and at the end of polymerization have unequal reaction conditions). Moreover, the vinyl groups of the different monomers involved and also the formed pendant double bonds often present distinct reactivities (see Fig. 15a). Cyclization reactions also occur to a great extent after incorporation of a multivinyl monomer (primary cyclization), increasing a lot the complexity of such cross-linking processes. These chemical effects can be magnified due to physical phenomena arising from the reaction of huge molecules with smaller polymer chains. These large molecules (see Fig. 15b) usually bear many pendant double bonds and radical centers, which can become inaccessible to further reaction due to steric hindrance.

Important deviations between predictions and measurements for vinyl/multivinyl radical copolymerizations were observed since the first works on this subject (e.g.,

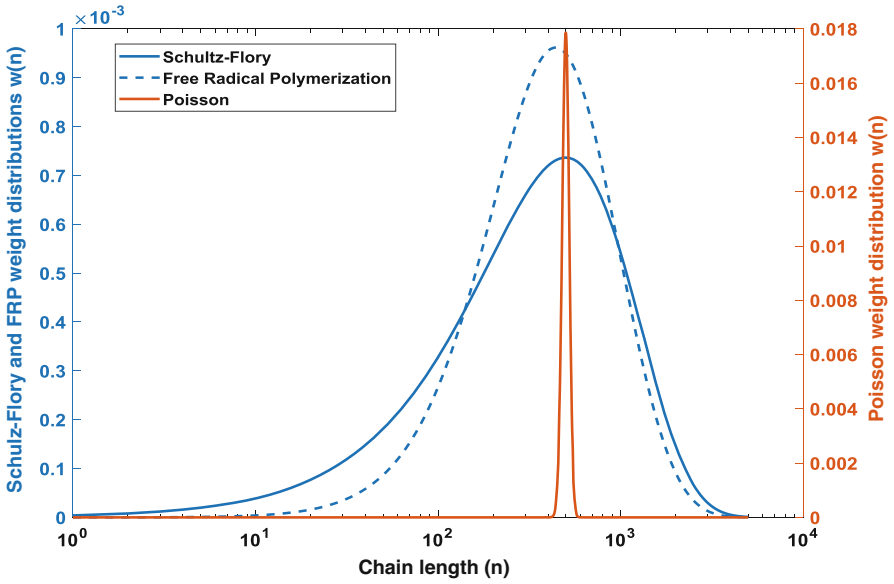

Fig. 11 Different kinds of weight chain length distributions ($w(n)$) considered in the simulations for the random cross-linking of primary chains arbitrarily distributed (see, e.g., Eq. (11)). With all the distributions the value $\bar{x}_n^* = 500$ was considered

much delayed gelation with respect to FS predictions was reported by Walling [34] when studying vinyl/divinyl copolymerization). Limitations of the statistical methods to describe nonlinear free radical polymerization, which is inherently kinetically controlled, stimulated the development of new modeling techniques. The first attempts to tackle branching by transfer to polymer are due to Beasley [40] and Bamford and Tompa [41]. In the latter approach [41], the solution of population balance equations (PBE) for polymer species was obtained through a continuous variable approximation in the Laplace domain. These ideas were at the origin of the nowadays called "method of the moments", allowing the description of kinetically controlled nonlinear polymerization systems when equal reactivity of functional groups holds.

Solution of the conservation laws for polymer species through a continuous variable approximation was considered by Zeman and Amundson [42, 43] along with several approximations to obtain a mathematically tractable problem. It is now deprecated given the use of appropriate numerical methods below described.

Kuchanov and Pis'men introduced important improvements in the kinetic theory of nonlinear polymerization in the early 1970s [44, 45]. Combination of PBE with generating functions and the solution of the resulting partial differential equations through the method of the characteristics allowed avoiding drastic approximation conditions used in precedent approaches. Avoiding the quasi-steady-state assumption for estimating radical concentrations and consideration of multiple active centers in the same molecule are decisive improvements introduced with the

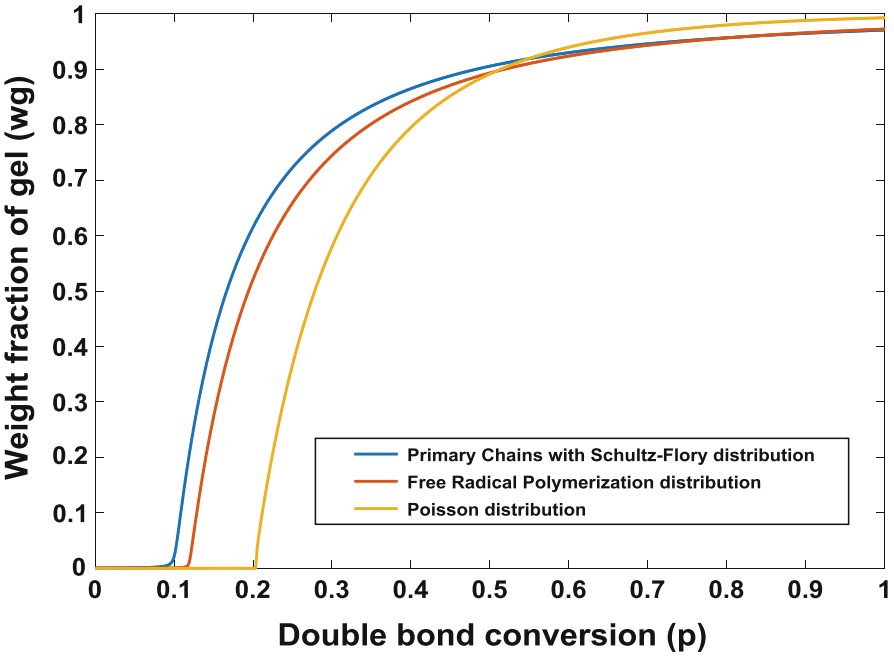

Fig. 12 Weight fraction of gel (w_g) as a function of the double bond conversion (p) in the random cross-linking of vinyl/divinyl monomers. Different kinds of weight chain length distributions for the primary chains ($w(n)$) were considered in these simulations ($\bar{x}_n^* = 500$ for all the distributions). Initial mole fraction of divinyl monomer $y_{DVM} = 0.5\%$ (y_f~1%)

Kuchanov and Pis'men works. Description of the post-gelation period is another important outcome of this kinetic theory.

In late 1980s, Tobita and Hamielec [46] introduced the pseudokinetic rate constant method to describe network formation in free radical polymerization. This method is based upon the use of moment equations, and the post-gelation period is described through the adaptation of Flory's cross-linking theory. The kinetic theory developed by Tobita and Hamielec [46] preserves the history of the generated network structure and allows a heuristic inclusion of primary and secondary cyclization. The simplicity of the numerical calculations involved makes this technique (often known as the Flory/Tobita (FT) model) very appealing for practical applications. The computations involve the instantaneous distribution of primary chains. In the framework of the pseudokinetic rate constant method, that distribution for a free radical process is described [46] by:

$$f_w(n,\theta) = \frac{n\alpha(\theta)}{(1+\alpha(\theta))^{n+1}}\left[\gamma(\theta) + 0.5\alpha(\theta)\beta(\theta)(n-1)\right] \tag{12}$$

With $\alpha(\theta) = \gamma(\theta) + \beta(\theta)$, $\beta(\theta) = k_{tc}R^{\bullet}/(k_pM)$, $\gamma(\theta) = (k_{td}R^{\bullet} + k_{fm}M + k_{fs}S)/(k_pM)$, and θ representing the birth conversion of the chains. In these equations k_p, k_{tc}, k_{td},

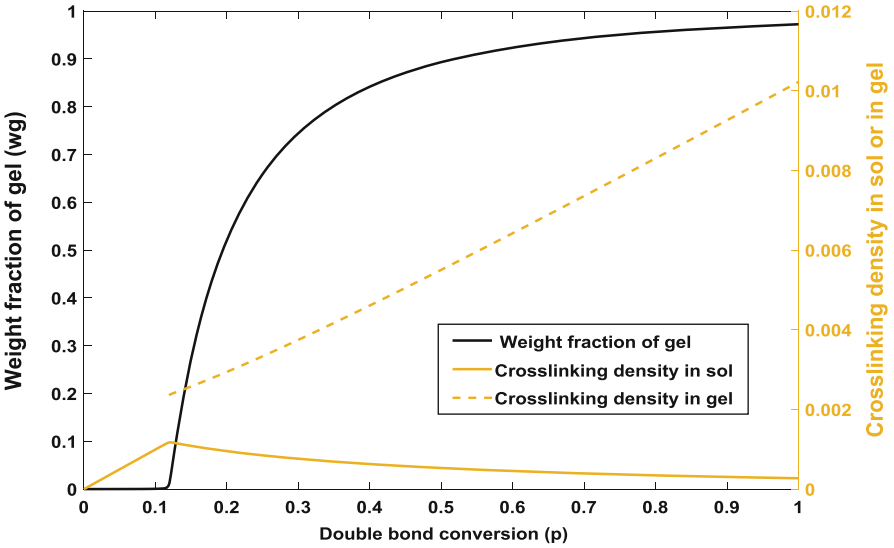

Fig. 13 Weight fraction of gel (w_g), cross-linking density of the sol (ρ'), and cross-linking density of the gel (ρ'') as function of the double bond conversion (p) in the random cross-linking of vinyl/divinyl monomers. The weight chain length distribution for the primary chains ($w(n)$) is correspondent to a polymer resulting from a free radical polymerization with $\bar{x}_n^* = 500$. Initial mole fraction of divinyl monomer $y_{DVM} = 0.5\%$ (y_f~1%)

k_{fm}, and k_{fs} stand for the pseudokinetic rate constants for propagation, termination by combination, termination by disproportionation, chain transfer to monomer, and chain transfer to solvent, respectively. On the other hand, M, $R^{\bullet}$, and S represent the total concentrations for monomer, radicals, and solvent, respectively.

The total cross-linking density at conversion ψ of the chains born at conversion θ in given by:

$$\rho(\theta,\psi) = \rho_i(\theta) + \rho_a(\theta,\psi) \tag{13}$$

The cross-linking densities and weight fraction of sol are calculated through:

$$\rho_i(\theta) = \frac{k_p^{*0}(\theta)[\bar{F}_2(\theta) - \overline{\rho}_a(\theta) - \overline{\rho}_c(\theta)]\theta}{k_p(1-\theta)} \tag{14}$$

$$\frac{\partial \rho_a(\theta,\psi)}{\partial \psi} = \frac{k_p^{*0}(\psi)[F_2(\theta) - \rho_a(\theta,\psi) - \rho_c(\theta,\psi)]}{k_p(1-\psi)} \tag{15}$$

$$w_s(\theta,\psi) = \sum_{n=1}^{\infty} f_w(n,\theta)[1 - \rho(\theta,\psi)(1 - w_s(\theta,\psi))]^n \tag{16}$$

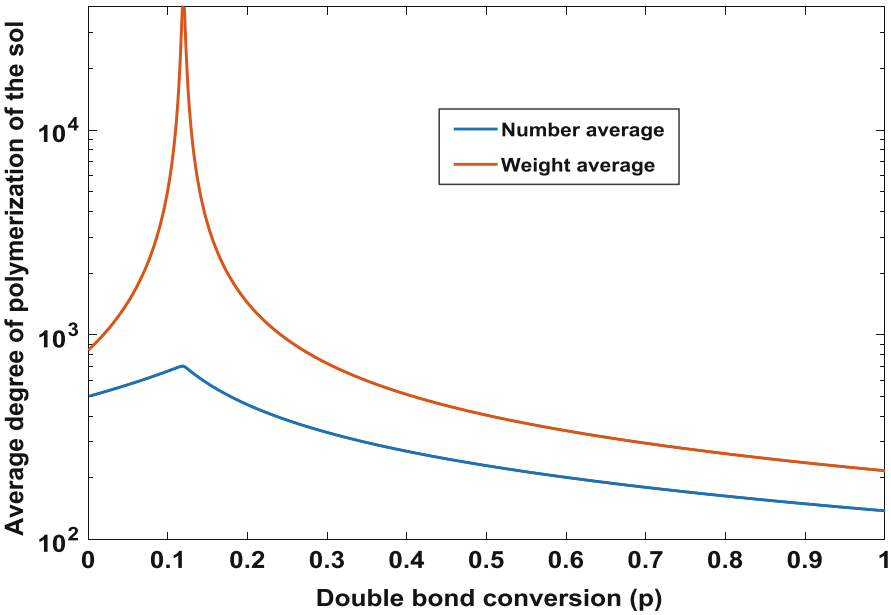

Fig. 14 Number- and weight-average chain lengths of the sol as function of the double bond conversion (p) in the random cross-linking of vinyl/divinyl monomers. The weight chain length distribution for the primary chains ($w(n)$) is correspondent to a polymer resulting from a free radical polymerization with $\bar{x}_n^* = 500$. Initial mole fraction of divinyl monomer $y_{DVM} = 0.5\%$ (y_f~1%)

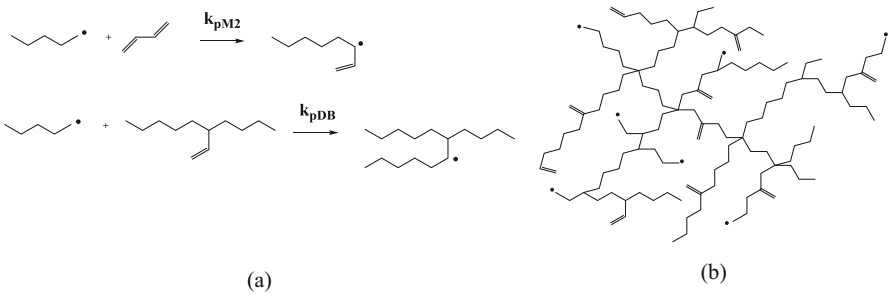

Fig. 15 (**a**) Depiction of divinyl monomer and pendant double propagation during a cross-linking process. (**b**) Large polymer molecule bearing many pendant double bonds and radical centers. Different reactivities of vinyl groups, intramolecular cyclization, and steric hindrance are examples of phenomena hampering the description of vinyl/multivinyl cross-linking systems

Details on the application of these equations and calculation methods with nonlinear free radical polymerization can be found in the original Tobita-Hamielec work [46].

The "numerical fractionation" technique was introduced by Teymour and Campbell in the 1990s [47]. This method splits the polymer population into an arbitrary

number of generations defined by a count of branching events and carries out the calculation of the moments for the polymer PBE in each generation. Transfer rules for transition of species between generations are defined. The average properties of sol and gel, as well as the chain length distribution (CLD) of the sol, can be obtained (note that the calculation of the sol CLD is not possible in the framework of the FT theory). Recently, the numerical fractionation technique was improved in order to take into account the existence in polymer population of multiradical species [48], a flaw in its original formulation. Note that modifications of the method of the moments for nonlinear FRP were also recently published [49].

This technique provides a heuristic approximation of polymer size distribution and its averages, but it is neither consistent nor convergent, in contrast with some well-based approaches, as discussed below.

5.4 Population Balances of Generating Functions

A general kinetic approach to describe different kinds of nonlinear irreversible polymerizations started to be developed in our research group in the 1990s [50]. This method stems from the ideas of Kuchanov and Pis'men [44, 45] and uses multidimensional generating functions to describe polymer populations. Through the use of a numerical approach for the solution of the resulting PBEs, several mathematical approximations inherent to alternative approaches can be avoided, namely, in nonlinear free radical polymerization processes [51]. Distinctive features of this approach comparatively to alternative methods, computation of different polymer molecular architecture parameters (CLD before and after gelation, weight fraction of gel, sequences, average radius of gyration), and its application to different kinds of polymerization systems (condensation, free radical polymerization, coordination polymerization, controlled radical polymerization) can be found elsewhere [50–61]. In a recent paper [62], the performance of four different modeling approaches (kinetic Monte Carlo, statistic/kinetic Flory/Tobita, PBE with generating functions, and PBE with numerical fractionation) was also compared in the framework of the bulk cross-linking copolymerization of vinyl/divinyl monomers.

The next case study highlights the use of population balance equations of generating functions to deal with hydrogels synthesis processes. Indeed, Eqs. (17, 18, 19, 20, 21, 22, 23, 24, 25, 26, 27, 28, and 29) depict a possible kinetic scheme describing a hydrogel synthesis (e.g., superabsorbent hydrogel) through the free radical copolymerization of an acrylic monomer (e.g., acrylic acid) with a cross-linker such as methylene bisacrylamide (MBAm, functionality $\alpha = 2$) or trimethylolpropane triacrylate (TMPTA, functionality $\alpha = 3$). In these equations, I, R_0, M_1, M_2, S, and Z stand for the initiator, primary radicals, acrylic monomer, cross-linker, solvent, and inhibitor, respectively. Polymer molecules ($P_{n,m}^{x,y}$) are described using a four-dimensional counting of radicals (n), pendant double bonds (m), polymerized acrylic units (x), and polymerized cross-linker units (y). Initiator (e.g., V50) decomposition is described through Eq. (17). Acrylic monomer, cross-

linker, and PDB initiations by primary radicals are depicted in Eqs. (18, 19, and 20). Propagations of acrylic monomer, cross-linker, and PDB with polymer radicals are shown in Eqs. (21, 22, and 23). Equations (24) and (25) represent chain transfer to acrylic monomer and to solvent, respectively. Inhibition is described through Eqs. (26) and (27) and termination by combination and by disproportionation by Eqs. (28) and (29), respectively.

$$I \xrightarrow{k_d} 2fR_0 \tag{17}$$

$$R_0 + M_1 \xrightarrow{k_{i1}} P^{1,0}_{1,0} \tag{18}$$

$$R_0 + M_2 \xrightarrow{k_{i2}} P^{0,1}_{1,\alpha-1} \tag{19}$$

$$R_0 + P^{x,y}_{n,m} \xrightarrow{k_{i3}} P^{x,y}_{n+1,m-1} \tag{20}$$

$$P^{x,y}_{n,m} + M_1 \xrightarrow{k_{p1}} P^{x+1,y}_{n,m} \tag{21}$$

$$P^{x,y}_{n,m} + M_2 \xrightarrow{k_{p2}} P^{x,y+1}_{n,m+\alpha-1} \tag{22}$$

$$P^{x,y}_{n,m} + P^{x\prime,y\prime}_{n\prime,m\prime} \xrightarrow{k_{p3}} P^{x+x\prime,y+y\prime}_{n+n\prime,m+m\prime-1} \tag{23}$$

$$P^{x,y}_{n,m} + M_1 \xrightarrow{k_{fm}} P^{x,y}_{n-1,m} + R_0 \tag{24}$$

$$P^{x,y}_{n,m} + S \xrightarrow{k_s} P^{x,y}_{n-1,m} + R_0 \tag{25}$$

$$R_0 + Z \xrightarrow{k_z} Inactive\ Products \tag{26}$$

$$P^{x,y}_{n,m} + Z \xrightarrow{k_z} P^{x,y}_{n-1,m} \tag{27}$$

$$P^{x,y}_{n,m} + P^{x\prime,y\prime}_{n\prime,m\prime} \xrightarrow{k_{tc}} P^{x+x\prime,y+y\prime}_{n+n\prime-2,m+m\prime} \tag{28}$$

$$P^{x,y}_{n,m} + P^{x\prime,y\prime}_{n\prime,m\prime} \xrightarrow{k_{td}} P^{x,y}_{n-1,m} + P^{x\prime,y\prime}_{n\prime-1,m\prime} \tag{29}$$

The general kinetic approach developed in our research group [50–61] uses generating functions (GF) of distributions instead of the related real domain functions. The GF of the distribution here used, $P^{x,y}_{n,m}$, is described by:

$$G(s_R, s_B, s_X, s_Y, t) = \sum_{n=0}^{\infty}\sum_{m=0}^{\infty}\sum_{x=0}^{\infty}\sum_{y=0}^{\infty} s_R^n s_B^m s_X^x s_Y^y P^{x,y}_{n,m}(t) \tag{30}$$

The population balance equation (PBE) for the kinetic scheme described by Eqs. (17, 18, 19, 20, 21, 22, 23, 24, 25, 26, 27, 28, and 29) in the Laplace domain is:

$$\begin{aligned}
\frac{\partial G}{\partial t} &= k_{i1}[R_0][M_1]s_X s_R + k_{i2}[R_0][M_2]s_Y s_R s_B^{\alpha-1} + k_{i3}[R_0]\left(\frac{s_R}{s_B} - 1\right)\frac{\partial G}{\partial \log s_B} \\
&+ k_{p1}[M_1](s_X - 1)\frac{\partial G}{\partial \log s_R} + k_{p2}[M_2]\left(s_Y s_B^{\alpha-1} - 1\right)\frac{\partial G}{\partial \log s_R} \\
&+ k_{p3}\left[\frac{1}{s_B}\frac{\partial G}{\partial \log s_B}\frac{\partial G}{\partial \log s_R} - [R]\frac{\partial G}{\partial \log s_B} - [B]\frac{\partial G}{\partial \log s_R}\right] \\
&+ k_{fm}[M_1]\left(\frac{1}{s_R} - 1\right)\frac{\partial G}{\partial \log s_R} + k_s[S]\left(\frac{1}{s_R} - 1\right)\frac{\partial G}{\partial \log s_R} \\
&+ k_Z[Z]\left(\frac{1}{s_R} - 1\right)\frac{\partial G}{\partial \log s_R} + k_{tc}\left[\frac{1}{s_R^2}\left(\frac{\partial G}{\partial \log s_R}\right)^2 - [R]\frac{\partial G}{\partial \log s_R}\right] \\
&+ k_{td}[R]\left(\frac{1}{s_R} - 1\right)\frac{\partial G}{\partial \log s_R}
\end{aligned} \tag{31}$$

Starting the polymerization from monomers, initiator, and solvent (and/or other non-polymeric species), the initial condition for Eq. (31) is:

$$G_{|t=0} = G_0 = 0 \tag{32}$$

Numerical inversion of the generating function can be carried out in a stable and accurate fashion through contour integration in complex plane.

This general kinetic approach is also able to deal with more complex kinetic schemes and models describing hydrogel formation, namely, intramolecular chain transfer to polymer, backbiting, or propagations with tertiary radicals [20]. These additional kinetic mechanisms should only be important at high polymerization temperature, very low cross-linker content, and high polymer concentration. Polymerization recipes for the formation of hydrogels from two vinyl monomers (e.g., acrylic acid and acrylamide) and a cross-linker can also be handled in the framework of this modeling approach [22].

Figure 16 illustrates the use of such a modeling approach with hydrogel synthesis. In Fig. 16a, it is presented the experimentally measured dynamics of gel formation in different polymerization runs concerning AA-based hydrogel production (inverse suspension processes). In Fig. 16b, it is compared the predicted and experimentally measured final weight fraction of gel for different polymerization runs concerning hydrogel synthesis. The effect of the reactivity of pendant double bonds on the predictions is here explored. In spite of the fair agreement between experimental and theoretical predictions, improvement of this modeling approach has been considered in the last few years, namely, taking into account cyclization effects [24, 63].

The prediction of the average molecular weight between cross-links ($\bar{M}_c$), an important parameter for the characterization of polymer networks, is also possible in the framework of the present modeling approach. Indeed, segments between cross-linking points can be treated as sequences of the main monomer present in the hydrogel. Methods for the calculation of sequence lengths in linear and nonlinear polymerization have been previously developed by our research group [56, 59] (see also [64] for a comprehensive overview on polymerization processes modeling, including the calculation of sequence length distributions).

5.5 Calculations with RDRP Nonlinear Polymerization

Due to the particular kinetic mechanisms involved, calculations with nonlinear RDRP systems have some numerical issues owing to their huge span of reaction times [60] and critical improvements on the above-described method based on

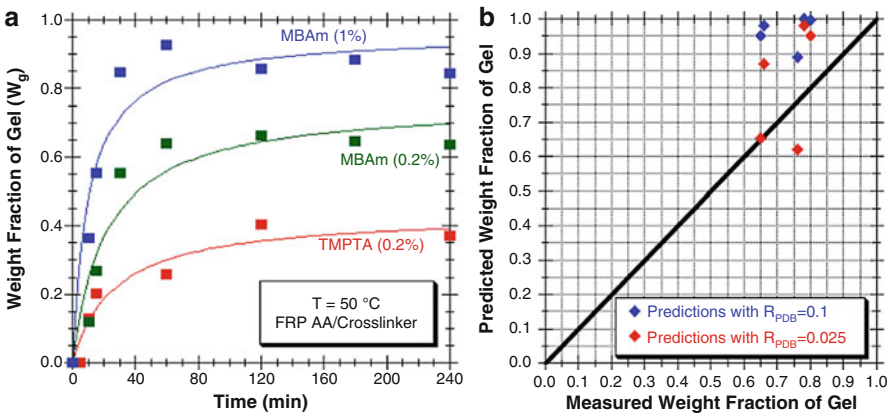

Fig. 16 (**a**) Experimentally measured dynamics of gel formation in AA-based hydrogels production. FRP polymerizations at T = 50 °C with different cross-linkers (MBAm and TMPTA) at different initial contents were considered. (**b**) Comparison of the measured and predicted final weight fraction of gel in different polymerization runs concerning the AA-based hydrogel formation. Predictions with two values for the reactivity of the pendant double bonds are presented

generating functions are being performed at the time this work is being completed. The increase of the efficiency of the numerical methods used with the solution of two-point boundary value problems involved in the calculations after gelation or in inversion of the CLD could overcome most of those issues (indeed, analysis of NMRP and ATRP nonlinear polymerization before gelation was previously performed in the framework of this approach [61, 65, 66]).

Other important tools can be found in the literature to deal with such kinds of problems, mostly based on adaptations of the method of the moments (see, e.g., [67, 68] and references therein). These calculation tools were recently explored for the development of RAFT-surface-grafted molecularly imprinted particles [25], and some useful simulations are illustrated in Fig. 17, namely, the control of the gelation process through the initial amount of RAFT agent (manipulation of the primary chains) and the CLD prediction with linear RAFT polymerization. Note that this kind of analysis is important for polymer networks and hydrogels tailoring, for design of telechelic structures, and also for RAFT-grafting processes, namely, those involving cellulose, as explored in Sect. 6.

6 Tailoring of Branched/Network Polymers and Hydrogels with RDRP Mechanisms

Reversible deactivation radical polymerization (RDRP), formerly named living radical polymerization (LRP) or controlled radical polymerization (CRP), offers the possibility to synthesize polymers with predetermined degree of polymerization and narrow molecular size distribution, tackling a major drawback of classical free radical polymerization (FRP) [69, 70]. Additionally, with RDRP, it is possible to carry out the synthesis of advanced polymer structures with tailored composition (e.g., block, statistical, gradient, or graft copolymers), architecture (e.g., linear, star, comb, network, or branched polymers), and functionality (e.g., telechelic polymers, macromonomers, multi-armed polymers, or multifunctional polymers). RDRP mechanism also provides the efficient production of molecular composites such as hybrids with inorganic and biopolymers, functional colloids, or modified surfaces [69, 70].

In this section are presented results for case studies concerning the tailoring of branched polymers, networks, and hydrogels through RAFT polymerization. The RAFT synthesis of hydrogel particles in continuous flow micro-reactor, the generation of molecularly imprinted particles with surface RAFT-grafted polymer brushes, and the RAFT-grafting of synthetic polymers in cellulose are considered as application examples. Note that, among the main RDRP mechanisms, RAFT polymerization presents some advantages due to the broad range of operation conditions and different classes of monomers that can be used [71]. This technique was also before considered in the cross-linking of different kinds of multi-olefinic monomers to generate polymer networks [72]. However, many similar applications are possible with other RDRP mechanisms, namely, ATRP and NMRP.

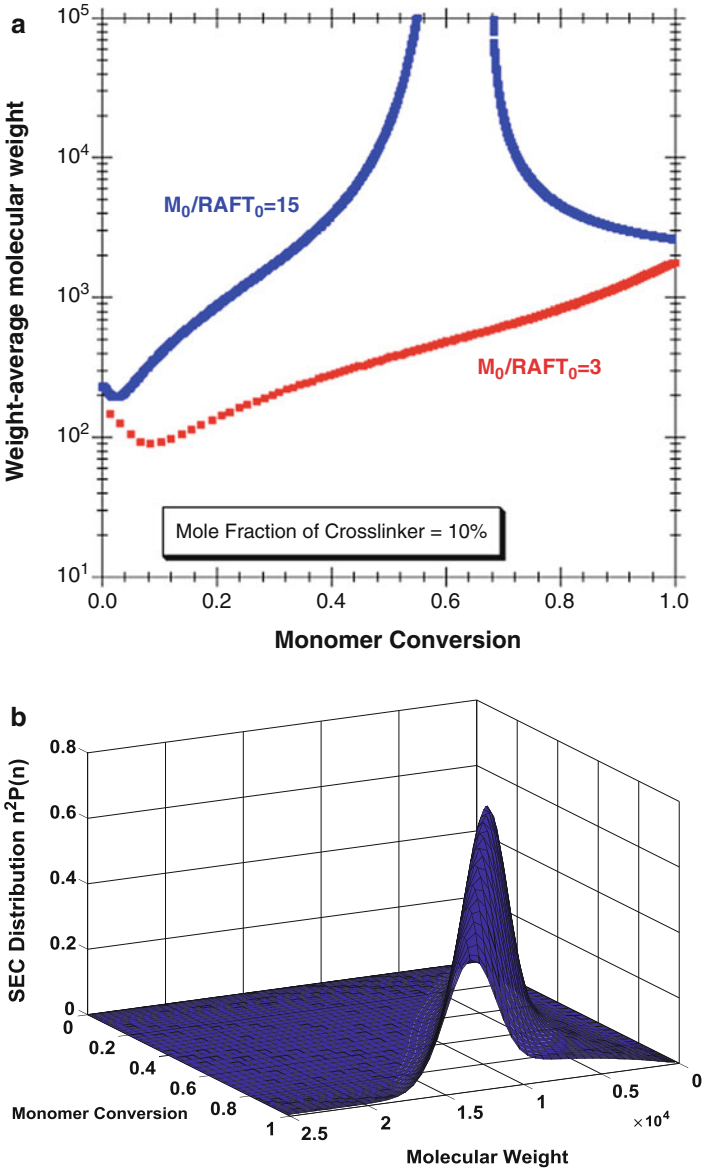

Fig. 17 (**a**) Predicted dynamics of HEMA/EGDMA hydrogel formation for processes with different initial contents of RAFT agent, showing the possibility to avoid gelation even at a high cross-linker content (see [25] for information concerning the relevant kinetic parameters). (**b**) Predicted dynamics of the CLD with the RAFT polymerization of MAA (see [68] for a general discussion concerning the influence of the kinetic mechanisms on the CLD of RAFT linear polymers, namely, the possibility for the development of bimodal distributions)

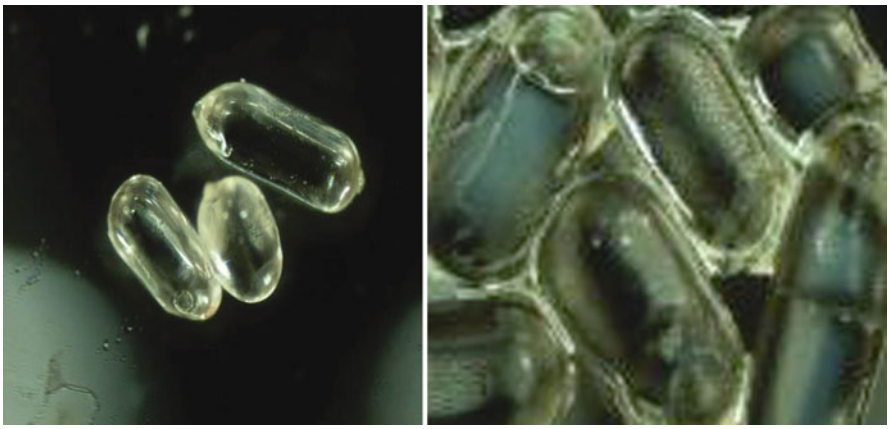

Fig. 18 Images of AA hydrogel particles synthesized in a continuous flow process. RAFT polymerization was considered to control the kinetics of the reaction and the gelation mechanism

6.1 Continuous Flow Synthesis of Hydrogel Particles with RAFT Polymerization

As pointed above, RDRP mechanisms offer the possibility for production of advanced polymer structures with tailored composition. These techniques can also be explored to try the synthesis of more homogeneous polymer networks (e.g., controlling the molecular weight between cross-links), as recently reported with RAFT polymerization [17]. Additionally, the control of the kinetics of polymerization and, eventually, the suppression of gelation (if the primary chains are sufficiently shortened) can also be conceived with these processes, as also recently described [73]. Here, it is illustrated the use of RAFT polymerization in our research to aid in the production of hydrogel particles in a continuous flow micro-reactor [74]. Indeed, it was shown that the inclusion of a RAFT agent in the developed process was important to optimize the experimental conditions in the continuous microfluidic approach. The control of the reaction kinetics, namely, the fast and exothermic reaction involving AA, was thus attained. Moreover, with RAFT polymerization, the gelation time could also be manipulated in this microfluidic approach and molecularly imprinted hydrogel particles were successfully synthesized [74]. In Fig. 18 are presented images of hydrogel particles obtained with such approach. The molecularly imprinted hydrogel particles obtained with this methodology (e.g., using 3-aminopyridine as template) also showed outstanding performance in a selective uptake process guided by the swelling of the networks [74]. These findings illustrate the use of RAFT to help the tailoring of smart hydrogels. Morphological features introduced in the hydrogels by using a microfluidic device will be further discussed in Sect. 7 of this work.

6.2 Network Polymer Particles with Surface RAFT-Grafted Functional Brushes

In the last few years, molecular architectures such as network polymer particles forming a core with surface-grafted functional polymer brushes have been explored to create materials with multiple features. A molecularly imprinted core, able to perform molecular recognition of a target molecule, bearing functional brushes grafted at the particle surface, is an example of such class of materials. The functional polymer brushes are included to provide stimulation features to the final materials and/or to modify their surface properties (e.g., hydrophilic/hydrophobic balance). A possible synthesis route of these kinds of functional materials includes two steps (see [75–80] and references therein): (i) production of network polymer particles using RAFT precipitation polymerization. A high cross-linker content is classically considered in this step if MIPs are intended. (ii) Grafting of functional polymer brushes on the core particles surface through a "grafting from" mechanism. With this goal, the RAFT groups present in the surface of the particles produced at the first stage are reactivated in this second polymerization step.

These ideas were recently explored in our research group to develop MIP particles for 5-FU (used in cancer treatment) with surface-grafted polymer brushes, aiming pH and temperature sensitivity [81]. Imprinted polymer networks based on the functional monomers MAA and HEMA, with EGDMA as cross-linker, were synthesized through RAFT precipitation polymerization in ACN. Functional brushes were afterward grafted on the surface of these MIP particles using alternatively MAA, HEMA, or NIPA as monomers. Improved sensitivity of the particles with PMAA polymer brushes to the pH of the surroundings was also proven, and a boost on drug release at 20 °C as compared to 40 °C was observed for particles with PNIPA grafted brushes [81].

Currently, we are exploring this approach to generate engineered materials for the selective uptake and release of polyphenols. These molecules are present in many vegetable extracts, and, due to their antioxidant activity, many important applications in pharmaceutics and biomedicine are being considered. In Fig. 19 are presented results concerning the batch adsorption of the polyphenol polydatin in MIP particles bearing different kinds of surface-grafted polymer brushes, namely, PMAA, PDMAEMA, and PNIPA polymers. These materials were synthesized considering the above-described RAFT process with 4VP as functional monomer for molecular imprinting and EGDMA as cross-linker. The RAFT-mediated "grafting from" mechanism was afterward considered for brushes formation at particles surface. Results presented in Fig. 19 illustrate the possibility for stimulation of the molecular recognition process through the effect of the grafted polymers (the effect of the temperature is here considered within this purpose). However, other phenomena should be considered in this analysis (e.g., the effect of pH and temperature on drugs solubility) in order to have a clear picture of these stimulated uptake/release mechanisms. Ongoing studies with these classes of materials should help to differentiate the intervenient phenomena.

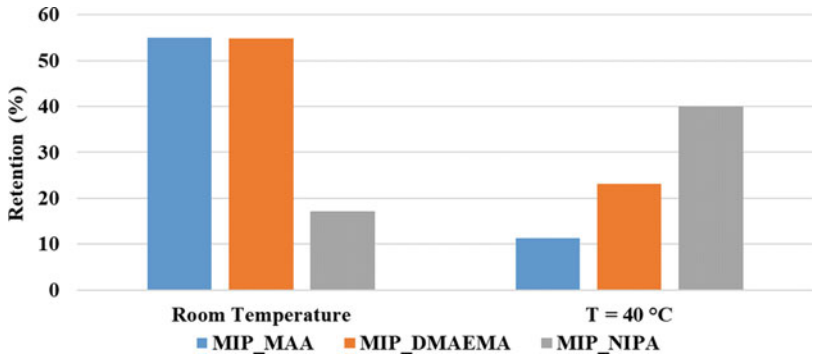

Fig. 19 Batch adsorption of polydatin in MIP particles bearing different kinds of surface-grafted polymer brushes, namely, PMAA, PDMAEMA, and PNIPA chains. Synthesis of these materials was performed through RAFT cross-linking precipitation of 4VP/EGDMA, followed by a RAFT-mediated "grafting from" process

Interestingly, the RAFT "grafting from" processes here briefly discussed have a close connection with the grafting of synthetic polymers on cellulose, as next discussed.

6.3 RAFT-Mediated Grafting of Synthetic Polymers on Cellulose

Grafting is a technique commonly used to modify the surface of many polymers. Grafting of cellulose is usually considered to improve the properties of the native natural polymer, such as water absorption capability, elasticity, hydrophilicity or hydrophobicity, adsorption features, sensitivity to external parameters (e.g., pH and temperature), antibacterial effect, etc. [82, 83]. Three main routes for grafting of cellulose are generally considered [82, 83]: (i) the "grafting from" approach consisting on the polymerization of a vinyl monomer in the presence of cellulose, whose backbone is also properly initiated for polymerization. Different methods can be used to initiate the polymerization in cellulose backbone including, e.g., the use of chemical initiators able to create radicals on cellulose or by the pre-attaching of a RAFT agent on cellulose followed by RAFT polymerization of the vinyl monomer. (ii) The "grafting to" or the "grafting through" approaches consisting on the reaction of a polymer containing reactive end groups with others present in cellulose backbone or the polymerization of a vinyl derivative of cellulose with a vinyl monomer. (iii) The "high-energy irradiation" approach where monomer and cellulose are mutually or separately irradiated.

A major challenge to be faced with cellulose grafting is due to the low solubility of this polymer in common solvents, which can hinder the reaction mechanisms involved in the grafting process. In practice, grafting of cellulose can be performed in homogeneous and heterogeneous conditions. With the homogeneous grafting, native cellulose is dissolved in a proper solvent (e.g., LiCl/DMAc), or a soluble cellulose derivative is used (e.g., hydroxyethyl cellulose or cellulose acetate). In

heterogeneous grafting, native cellulose and common solvents are directly used, and the process takes place only in the accessible regions of the polymer backbone. As a consequence of these effects, a higher grafting efficiency is ascribed to the homogeneous processes [82, 83].

In view of the ecologic/economic importance of cellulose valorization and in result of the challenges briefly described above, there is an intensive research effort on the improvement of the cellulose grafting methods and exploitation of the resulting materials (see [82–88] and references therein).

Here, we present results of our research concerning the grafting of different kinds of synthetic polymers on cellulose, using the "grafting from" approach mediated by RAFT polymerization in heterogeneous conditions. The accomplishment of this task with some of the conditions considered is also shown.

Three different kinds of cellulose were used in the studies performed, namely, cellulose fibers, cellulose microcrystalline, and cellulose filter paper (see Sect. 2). TBTGA and CPA were selected as RAFT agents containing carboxylic acid functional groups. Immobilization of RAFT agents on the cellulose substrates was performed through the esterification reaction of the acidic groups with the hydroxyl groups of cellulose, following the lines of thought reported in the literature (see [83–87] and references therein). DCC and DMAP were used as coupling agent and catalyst, respectively, for the esterification reaction. Note that, RAFT agents can be attached to cellulose via the R-group approach or the Z-group approach [83–87]. Here, the R-group approach was considered, resulting in the formation of a cellulose-supported macrochain transfer agent. Different esterification conditions were tried, namely, by combining the three types of cellulose and the two RAFT agents in three different solvents, specifically, DCM, DMF, and chloroform, following diverse alternatives also reported in the literature [83–87]. All the esterification reactions were performed at 40 °C during 3 days. Afterward, the cellulosic materials were submitted to intensive cleaning procedures [83–87] in order to remove the RAFT molecules without chemical bound to the substrates. Final purified products were dried in a vacuum oven at 40 °C.

The heterogeneous grafting of synthetic polymers on the cellulose was performed using the previously prepared cellulosic materials with attached RAFT agents and DMF as solvent for polymerization reaction. Different monomers were used in the grafting process (e.g., MAA and styrene), AIBN was selected as thermal initiator, and the same RAFT agent attached to the cellulose was considered in the polymer grafting step. All the reactions were performed at 70 °C during 24 h under stirring. The concentration of esterified cellulose in DMF was typically $P = 3$ g/L. Initial concentrations for monomer, initiator, and RAFT agent used in the grafting processes were typically $M_0 = 0.9$, $I_0 = 6 \times 10^{-3}$, and $RAFT_0 = 7.5 \times 10^{-3}$ mol/L, respectively. At the end of the reactions, the solid products and the liquid phase were separated using centrifugation. The presence of soluble polymer in the liquid phase was visually confirmed through the precipitation of a few drops in a large excess of a suitable non-solvent (such as diethyl ether or methanol). The collected liquid phase was stored at low temperature to be later analyzed, namely, using SEC. Solid materials were extensively cleaned considering several extraction processes, and

the final grafted cellulose was obtained through the drying of the products in a vacuum oven at 40 °C.

In Figs. 20 and 21 are presented some results concerning the FTIR analysis of different materials involved in the RAFT-mediated grafting of synthetic polymers on cellulose. For illustration purposes, the TBTGA-mediated grafting of PMAA on microcrystalline cellulose and the CPA-mediated grafting of PS, also on microcrystalline cellulose, are here presented. The comparison of the spectra correspondent to the synthetic polymer (PMAA or PS), the native cellulose, the cellulose substrate with esterified RAFT agent, and the final products of the grafting processes, allows to conclude that the intended cellulose-grafted materials were successfully obtained. Indeed, new FTIR assignments can be clearly identified in the grafted materials in the region 1550 to 1750 cm^{-1}. These new assignments, negligible in the native cellulose or in the correspondent substrate with attached RAFT agent, are compatible with vibrational features associated with the synthetic polymers, namely, the carbonyl C=O stretch (generically in the range 1670 to 1820 cm^{-1}) for PMAA and the aromatic C=C bending (generically in the range 1500 to 1700 cm^{-1}) for PS. In fact, the new assignments observed in the region 1550 to 1750 cm^{-1} for the cellulose-grafted materials can be closely related with vibrational peaks also appearing the spectra collected for the PMAA and PS polymers (see Figs. 20 and 21).

In Fig. 22 are presented results concerning the SEC analysis of the liquid phase correspondent to different grafting processes. These analysis were performed using DMF as eluent in order to have simultaneous solubility of different polymers, namely, PMAA and PS. Note that the same solvent was used in graft polymerization processes in order to keep the formed free polymer soluble during the reaction. These analyses provide an additional evidence for the formation of free polymer (first confirmed through the precipitation in a non-solvent, as above described) and allow to characterize the synthetic polymer population produced. With the two systems selected to illustrate these issues (PMAA and PS RAFT-grafting on cellulose), important differences can be identified with the SEC analysis of the liquid phase. Indeed, for PMAA grafting a unimodal polymer population is observed (with maximum RI intensity at around 8×10^4 molecular weight), while for PS grafting a bimodal distribution is measured (with maximum RI intensities at 4×10^3 and 8×10^4 molecular weight). Moreover, with MAA RAFT polymerization, the monomer peak is not observable in the final liquid phase, while a peak with substantial intensity is measured with S RAFT polymerization at the same conditions. The rates of consumption of the two monomers in these systems are therefore quite different. These issues highlight the important dissimilitudes possibly arising when variable RAFT-grafting systems are considered. In this context, modeling tools for RAFT polymerization, as described in Sect. 5, can provide interesting insights concerning the impact of kinetics, the operation conditions, and some mechanistic effects (e.g., the intermediated radical termination process and bimodality [68]) on the structural features of the formed polymer.

Our current research work in this field aims at the use of cellulose-grafted materials, such as those described above, for the generation of sorbents and controlled release vehicles [88], namely, molecularly imprinted polymers based on

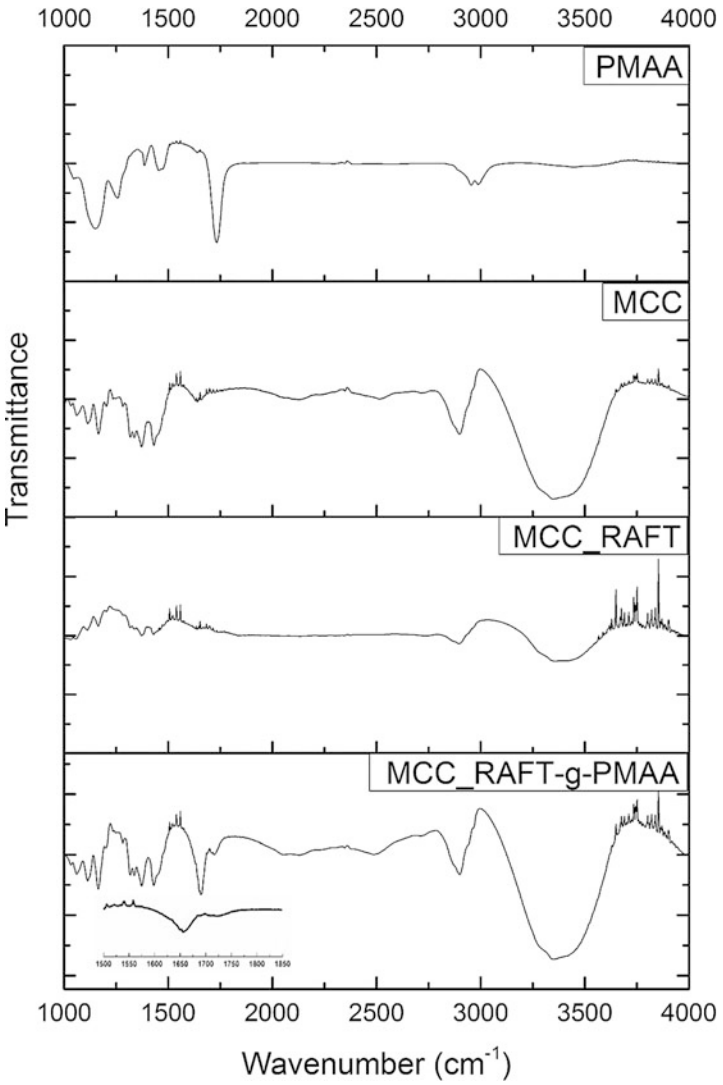

Fig. 20 FTIR spectra of different products involved in the RAFT-mediated grafting of PMAA on microcrystalline cellulose. Spectra collected for the PMAA polymer, microcrystalline cellulose (MCC), product of the esterification of microcrystalline cellulose with TBTGA (MCC_RAFT), and final product for the RAFT-grafting of PMAA on cellulose (MCC_RAFT-g-PMAA) are compared

natural macromolecules. Indeed, through the grafting of functional polymers in cellulose, improved interactions with selected template molecules can be conceived for an efficient molecular imprinting process. The ulterior generation of a polymer network, using a RAFT cross-linking mechanism with a divinyl monomer, e.g., leads (hopefully) to a MIP with molecular recognition capabilities for the template molecule, as generically depicted in Fig. 23.

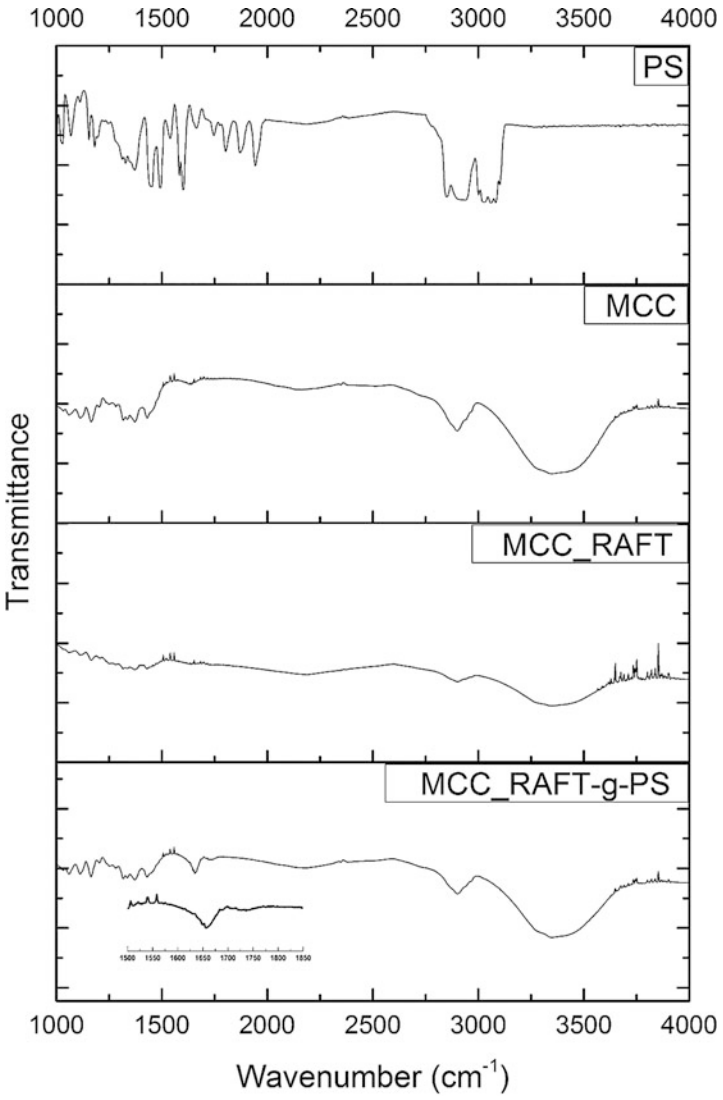

Fig. 21 FTIR spectra of different products involved in the RAFT-mediated grafting of PS on microcrystalline cellulose. Spectra collected for the PS polymer, microcrystalline cellulose (MCC), product of the esterification of microcrystalline cellulose with CPA (MCC_RAFT), and final product for the RAFT-grafting of PS on cellulose (MCC_RAFT-g-PS) are compared

However, some key aspects of the different synthesis steps are being worked out in order to achieve this final goal. Improvement of the RAFT-mediated grafting on cellulose, aiming higher efficiency and upper control on the molecular size of the synthetic functional chains, is an important issue in this context. The homogeneous RAFT-grafting process is a different approach being considered in our research. The

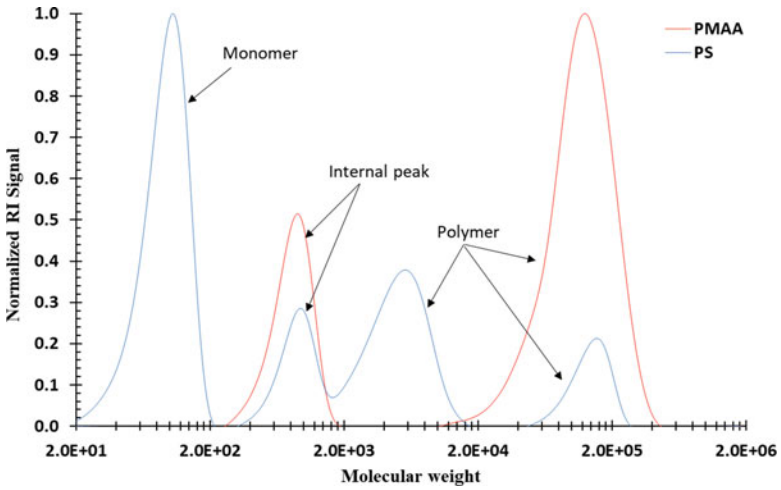

Fig. 22 SEC analysis for the final liquid-phase correspondent to the RAFT-mediated grafting of PMAA and PS on the microcrystalline cellulose. The analyses were performed using DMF as eluent at 0.4 mL/min and T = 35 °C. Polystyrene standards were used to calibrate the relation molecular weight versus elution volume

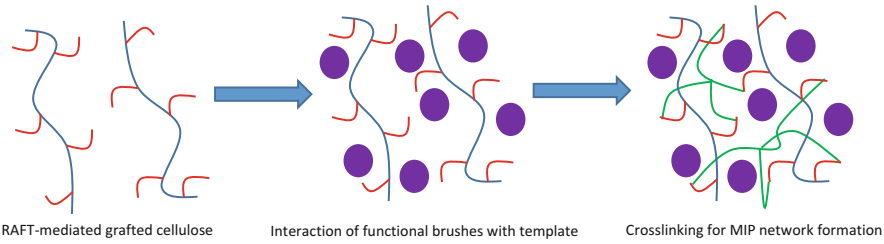

Fig. 23 Depiction of a possible molecular imprinting process based on the use of RAFT-mediated grafted cellulose and a RAFT cross-linking mechanism

favorable conditions for the formation of a polymer network in the final imprinted materials are also being investigated. A RAFT polymerization in the presence of a multifunctional vinyl monomer is being used as starting point.

7 Changing of Materials Morphology and Surface Modification

In many applications, end-use performance of polymer network-based materials and hydrogels strongly depends on mass transfer phenomena. On other hand, these transport mechanisms rely on the morphology, porosity, and surface properties, e.g., of the materials. Swelling ability and sorption/desorption capacity are examples

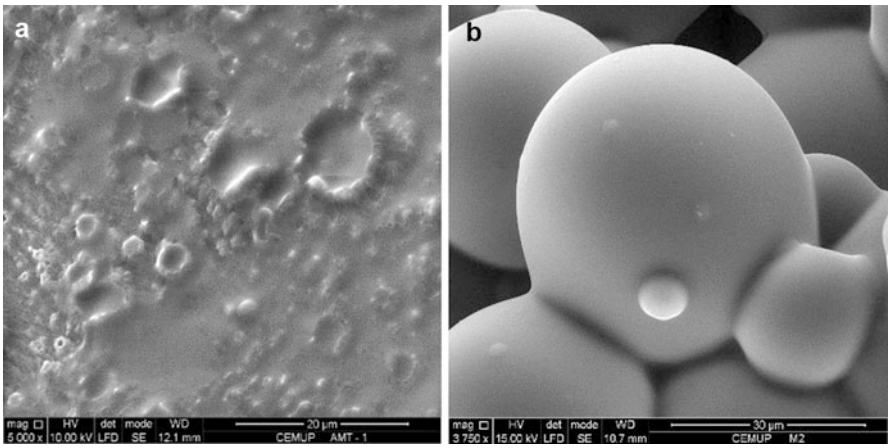

Fig. 24 SEM micrographs of AA/MBAm hydrogels produced through solution free radical polymerization process (**a**) and inverse suspension (**b**)

of important properties of polymer network materials and hydrogels that are changed by their morphology and physicochemical features.

The reaction process used in a polymerization system is an important engineering tool that can be explored to aid in the tailoring of the produced materials. Reactor type (e.g., batch, continuous, etc.) and the alternative use of solution, bulk, suspension, inverse suspension, and emulsion polymerization are examples of process variations with important impact on the morphology and final properties of polymers. Different approaches can also be used to change physicochemical characteristics of the materials, namely, their surface properties. A reaction process making use of functional groups present in the native polymers is a possible route to achieve this goal. In this section we illustrate the use of different reaction processes to change the morphology and the performance of hydrogels and SAPs. The surface modification of the materials, also impacting their applications, is highlighted with the change of the physicochemical properties of cellulose through a cross-linking process.

7.1 Polymerization Processes to Tailor Products Morphology

In Figs. 24, 25, and 26 are presented examples of different morphologies for hydrogels and polymer network products addressed in our research activities. The SEM micrograph for an AA/MBAm hydrogel produced through solution polymerization is presented in Fig. 24a. A continuous material is generally obtained in such conditions. Milling and sieving of the polymer networks is usually performed in order to enhance the mass transport properties and to control particle size. At the expense of a more complex chemistry, possibly introducing undesirable chemicals, hydrogel particles can be obtained using an inverse suspension process (see also [21, 22]). Particles in the range of few micrometers can thus be produced (see Fig. 24b),

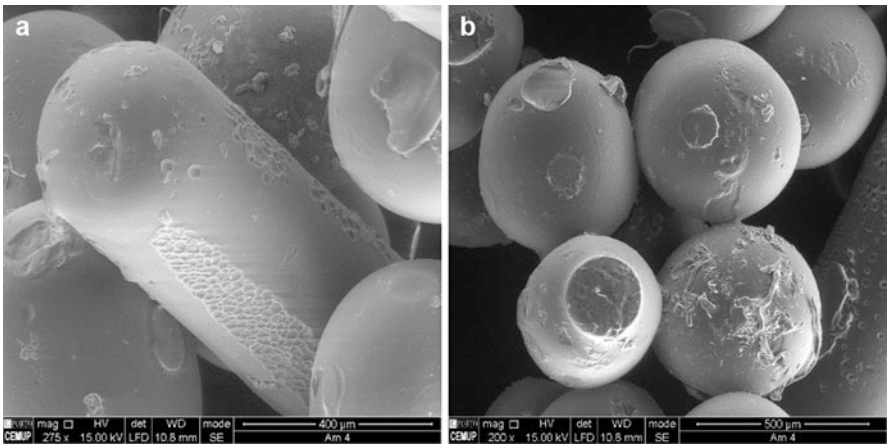

Fig. 25 SEM micrographs of AA hydrogel particles produced in a continuous flow micro-reactor. (**a**) Axial view of the cylindrical hydrogel particles. (**b**) Top view of the hydrogel particles

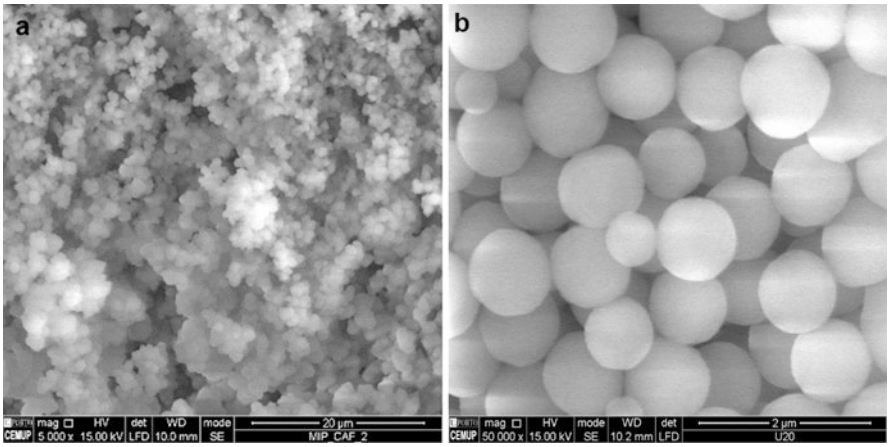

Fig. 26 (**a**) SEM micrograph of caffeine molecularly imprinted particles produced through inverse suspension. (**b**) SEM micrograph of polydatin molecularly imprinted particles produced through precipitation polymerization

and the process conditions (continuous to disperse mass ratios, surfactant concentration, etc.) can be considered in order to manipulate the particle size. Fast swelling of such materials is usually observed, as previously shown in Sect. 3 of this work.

Operation in microfluidic reactors [74] is a possible route to produce hydrogel particles, avoiding the use of some chemicals inherent to inverse suspension (intensive cleaning of the materials is usually needed with this approach) and providing additional possibilities to control the size and the shape of the products. Examples of such kinds of morphologies are presented in Fig. 25. The huge swelling capacity of

these hydrogel particles triggered by a molecular recognition mechanism put into evidence the distinct features that can be obtained with this class of materials [74].

Molecular recognition capabilities and imprinting efficiency of molecularly imprinted polymers (see also Sect. 8 of this work) are strongly dependent on their synthesis process and final product morphology (see also [81, 89] and references therein). In Fig. 26 are presented SEM images correspondent to two different products obtained in this context by using differentiated polymerization approaches. Figure 26a is correspondent to a caffeine MIP produced through inverse suspension [89]. High performance of such particles, namely, as chromatographic packings, was observed [89]. Note that a kind of surface molecular imprinting process, guided by the inverse suspension conditions, should be an important contribution for the molecular recognition capabilities of these particles. SEM images for a polydatin MIP produced through precipitation polymerization are presented in Fig. 26b. Individual particles of very small size (in the microscale or nanoscale if desired) can be produced with this technique, which enhances the mass transfer mechanisms. Moreover, the surface grafting of polymer brushes in these particles can be readily performed (e.g., using a RAFT-mediated process). Introduction of stimuli-responsive features and surface modification are possible advantages of such approach [81].

7.2 Cross-Linking of Cellulose to Modify Physicochemical Properties

Recently, many studies addressed the synthetic modification of cellulose to improve physicochemical properties, namely, the dispersion capacity, hydrophobicity, and biocompatibility (see [90] and references therein). Chemical cross-linking of cellulose is pointed out as a facile route to improve the adsorption capabilities and hydration of the native polymer in consequence of the change of the surface area and related chemical properties [90]. Considering these possibilities, and in view of the development of cellulose-based adsorbents for polyphenols, we illustrate here simple studies concerning the cross-linking of cellulose with epichlorohydrin and the assessment of the resulting materials. The sorption capabilities of the generated cellulose-based materials in comparison with synthetic MIPs specifically designed to target polyphenols are also briefly discussed.

Cross-linking of cellulose with epichlorohydrin was performed following the procedures reported in the literature [90]. In a typical experiment, 2 g of cellulose fibers (medium, cotton linters) was heated under stirring in 16 mL of a 2 M NaOH aqueous solution at 80 °C during 3 h. Argon was used to provide an inert atmosphere in the vessel. Afterward, 1 mL of epichlorohydrin was dropwise added to the mixture, which was kept at 80 °C under stirring during 12 h to promote the cross-linking process. Finally, the products were neutralized with an HCl solution (1 M), and several cleaning steps were performed to isolate the cross-linked cellulose, as described in the literature [90].

A simple evidence for the modification of the physicochemical properties of the cellulose was obtained by submitting the native and cross-linked materials to the alkali/urea method for dissolution in aqueous systems, with cycles of cooling and thawing [7–9], as described in Sect. 3. In Fig. 27 are presented images of the resulting mixtures, showing the total dissolution of the native cellulose and the total insolubility of the modified polymer.

In Fig. 28 are presented results for the SPE retention of polydatin in the native cellulose fibers, in the modified fibers, and in an inverse suspension synthesized polydatin-molecularly imprinted polymer based on 4VP/EGDMA. A 0.02 mM polydatin solution in ACN/MeOH was used to carry out these studies. Measurements here performed put into evidence the superior performance of the specifically designed MIP for the polyphenol uptake comparatively to the cellulose-based

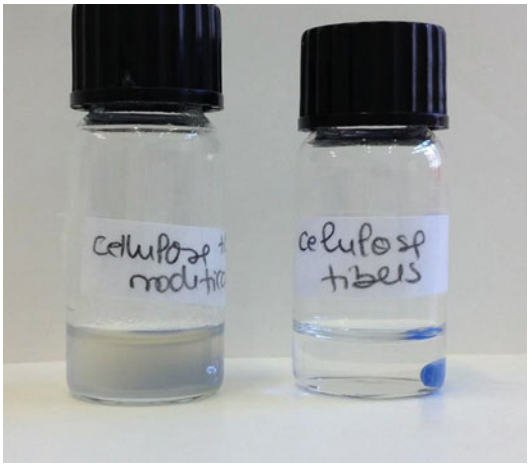

Fig. 27 Images for the mixtures resulting from the dissolution procedures applied to the epichlorohydrin-modified cellulose (left) and the unmodified cellulose (right). Following the alkali/urea method for dissolution of cellulose in aqueous systems with cycles of cooling and thawing, total dissolution was observed for the native cellulose, but the modified polymer remained totally insoluble

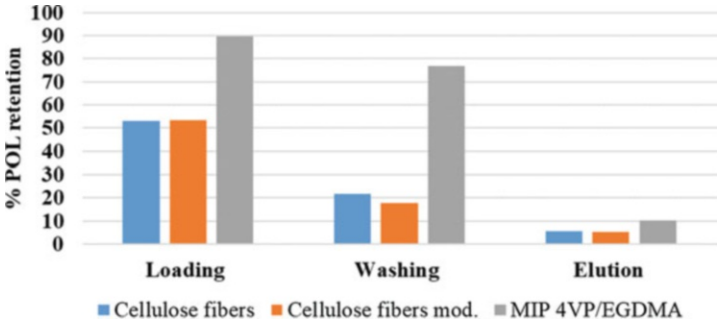

Fig. 28 Results for the SPE retention of polydatin in different sorbents, namely, the native cellulose fibers, the modified fibers, and in an inverse suspension synthesized polydatin-molecularly imprinted polymer based on 4VP/EGDMA. These testing conditions concern the loading of a 0.02 mM polydatin solution in ACN/MeOH (10/1), washing with the same eluent and elution with pure MeOH

sorbents. However, a relatively high retention is observed with both cellulose adsorbents (c.a. 50% retention). These results indicate that the benefits of cellulose modification on the polydatin retention capability are negligible, but some advantages on the use of the cross-linked cellulose can be conceived. Indeed, when the use of these cellulose polymers in continuous adsorption processes is sought, namely, as packing materials, the hardening and insolubility achieved with the cross-linking process are useful (e.g., avoiding the backpressure problem observed with some packing materials). The application of the modified cellulose as packing materials for polyphenol retention is currently being addressed in our research group.

Note that only a simple modification of cellulose for polyphenols adsorption was here discussed but more complex approaches can be considered within this purpose. Indeed, through the grafting of functional brushes on cellulose (e.g., using the RAFT-mediated processes discussed in Sect. 6), more specific interactions between the polyphenols and the adsorbent can in principle be created (e.g., including acidic or amine functional groups in the brushes). Additionally, the formation of a MIP network based on cellulose can also be thought, as depicted in Fig. 23, Sect. 6. In a different perspective, the analysis of the adsorption of polyphenols in cellulose is an important issue nowadays to understand the bioavailability of these antioxidant molecules, their metabolism, and pharmacokinetics [91].

8 Molecularly Imprinted and Non-imprinted Vehicles for Uptake and Controlled Release

Many polymer networks are designed to perform as vehicles for uptake and controlled release of target molecules. Here we illustrate the use of two very different systems within this general purpose. Molecularly imprinted polymers (MIPs), classically synthesized with a very large content of cross-linker to assure geometrical stability of the binding sites, and hydrogels, lightly cross-linked materials designed to allow swelling/shrinking induced mechanisms, are considered to highlight these differences.

8.1 Molecular Recognition with Molecularly Imprinted Polymers

Molecularly imprinted polymers (MIPs) play the role of artificial antibodies and are based on the creation in a polymer network of tailor-made cavities having high specificity and affinity with respect to a specific target molecule [92–94]. Nowadays, an intense research activity on MIPs is observed due to the important applications of these materials in many kinds of separations, solid-phase extraction, sensors, catalysis, and many biological processes (e.g., controlled drug delivery) [94, 95].

Classically, MIPs are produced with a very large content of a cross-linker plus a functional monomer, able to create specific interactions with the target molecule. After network formation, the binding sites formed should preserve the geometrical stability in order to uptake and release the target molecule in several cycles. Thus,

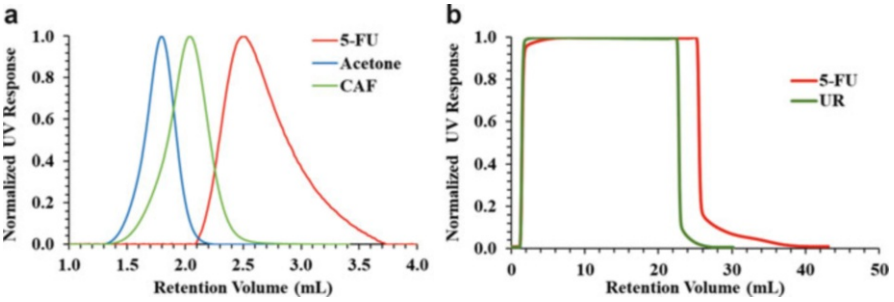

Fig. 29 Application of 5-FU MIP particles based on MAA/EGDMA, obtained by inverse suspension, as column packing for continuous adsorption/desorption processes: (**a**) chromatographic elution of 5-FU, caffeine, and acetone using ACN as eluent. (**b**) Uptake and release of 5-FU and UR in a frontal analysis process. A 50/4.6 length/diameter mm/mm column was used in these experiments

swelling is (in principle) almost unwanted with MIPs. However, performance of MIPs is affected by several factors concerning their preparation (chemical composition, polymerization process, morphology, etc.) and also their application (e.g., hydrophilic/hydrophobic interactions with the solvents considered). Therefore, there is plenty of room to develop new MIPs and improve their performance. MIPs for aminopyridines with swelling-induced molecular recognition [74], molecular imprinting of caffeine, and 5-FU in different kinds of particles (e.g., with inverse suspension or precipitation polymerization) [89] and RAFT-surface grafting of functional brushes in MIP particles to improve stimulation [81] are some recent activities of our research group in this area. Development of MIPs to address the uptake/release of polyphenols is another ongoing task, as before described in Sect. 7 of this work.

In Fig. 29 is illustrated a potential use of MIP particles in molecular recognition processes. 5-FU MIP particles based on MAA/EGDMA were synthesized by an inverse suspension process and packed in a small GPC column for assessment in continuous processes applications. Clear molecular recognition capabilities of the produced materials for 5-FU are evidenced in the chromatographic elution test (acetone and caffeine were considered as alternative molecules) and also in the frontal analysis experiment where the structural analogue uracil was also used. Note that ACN was used as eluent in these experiments and very different results can be obtained if other eluent is considered, such as water, due, e.g., to the role of the hydrophobic interactions [89]. Controlled swelling and morphological features of these particles are also important issues to avoid backpressure problems with continuous operation.

8.2 Swelling-Induced Controlled Release: A Case Study with Cellulose Hydrogels

Hydrogels are appealing controlled release vehicles due to their ability to control the transport of molecules in the network matrix. Additionally, as a consequence of their

high swelling capacity, biocompatibility, biodegradability, and biological functions, hydrogels based on natural polysaccharides, like cellulose, find many interesting applications in biomedicine, pharmacy, cosmetics, or food industry [5–9]. However, in order to design materials for accurate controlled release processes, the specific mechanisms intervenient in the transport of the target molecules inside the hydrogels should be known. Thus, important mathematical tools were developed in this research field in order to understand and develop tailored controlled release vehicles based on hydrogels [96–102].

For non-swellable devices, in the form of a thin polymer film, where the one-dimensional release of a solute from a slab applies, the following solution of the second Fick's law describes the amount $M(t)$ released along at time t:

$$\frac{M(t)}{M_\infty} = 1 - \sum_{n=0}^{\infty} \frac{8}{(2n+1)^2\pi^2} \exp\left[-\frac{D(2n+1)^2\pi^2}{L^2}t\right] \tag{33}$$

M_∞ in Eq. 33 is the amount of solute released when time approaches infinity and D the diffusion coefficient of the solute in the polymer matrix. A slab of thickness L, initially at uniform constant concentration of solute C_0 and which surfaces are kept along the time at constant concentration C_S, is here considered as model diffusion system [96, 101]. Solutions for analogue problems with cylinders or spheres can be obtained [96, 101]. Note that the solution presented in Eq. (33), as well as the equivalent solutions for cylinders and spheres (see [96, 101] for details on the solutions for these geometries), is independent of C_0 (which defines the initial condition) and C_S (which sets the boundary conditions at the slab surfaces).

In order to simplify the interpretation of experimental data obtained for the drug release in different devices, the empirical equation below was introduced by Ritger and Peppas [96]:

$$\frac{M(t)}{M_\infty} = kt^n \tag{34}$$

The above relation was shown to hold for the initial 60% of the release curve and to be valid for non-swellable vehicles with different geometries. The use of this equation was also extended to swelling-controlled release systems, namely, those prepared by incorporation of a drug in a hydrophilic glassy polymer, as long as a moderate equilibrium swelling ratio is observed (not higher than 1.33) [97].

The picture becomes much more complex with swellable-controlled release devices because the penetrant component (generally water) as soon as it gets into the polymer network also modifies its rate of drug release. Coupling of diffusion with macromolecular relaxation is generally observed and the transport of the drug outward the hydrogels is affected by the magnitude of these two phenomena. Modeling of such processes belongs to the general class of problems known as moving boundary problems or Stefan-Neumann problems (see [97–99] and Chap. 13 in Ref. [101]) and only numerical solutions are usually possible (see also [102] for a comprehensive view of hydrogels modeling). However, a heuristic model

developed by Peppas and collaborators [98] can fit the experimental data and thus allows the estimation of the contribution of the diffusion and relaxation mechanisms for anomalous drug release. It should also be stressed that phase equilibria and convective transport play an important role on drug uptake and release mechanisms in hydrogels, namely, at the boundary layer between the liquid phase and the insoluble polymer phase. Mass balance equations for the two phases should be solved in these circumstances, as depicted below for a hydrogel slab immersed in a liquid:

Hydrogel phase:

$$\frac{\partial C_A^H}{\partial t} = D_A \frac{\partial^2 C_A^H}{\partial x^2} \tag{35}$$

With initial and boundary conditions:

$$t = 0, -L/2 \le x \le L/2, C_A^H = C_{A0}^H$$

$$t > 0, x = \pm L/2, -D_A \left.\frac{\partial C_A^H}{\partial x}\right|_{x=\pm L/2} = k_c\left(C_A^{L*} - C_A^L\right) \tag{36}$$

Liquid phase:

$$\frac{dC_A^L}{dt} = k_c\left(C_A^{L*} - C_A^L\right) a_v \frac{V_H}{V_L}$$

$$t = 0, C_A^L = C_{A0}^L \tag{37}$$

In these equations, C_A^H and C_A^L represent the concentration of the drug in the hydrogel and liquid phase, respectively, L is the thickness of the slab, k_c the convective mass transfer coefficient between the two phases, and a_v is the surface area per unit of volume in the hydrogel. V_H and V_L represent the volumes of hydrogel and liquid in the system, and it is considered that the partition of the drug between the two phases is expressed by the coefficient $K = \frac{C_A^H\big|_{x=\pm L/2}}{C_A^{L*}}$. Thus, C_A^{L*} represents the concentration of the drug in the liquid phase that is in equilibrium with the surfaces of the hydrogel slab.

In Figs. 30 and 31 we present the analysis of experimental data for the uptake and release of the polyphenol polydatin in cellulose-based hydrogels (their synthesis with epichlorohydrin was presented in Sect. 3). Note that the understanding of the positive and negative biomedical interactions of polyphenols with cellulose [91] is being addressed in the scientific community because cellulose-based materials are potential vehicles for their controlled release [9].

The fraction of mass uptake during the impregnation of two different cellulose-based hydrogels with polydatin is presented in Fig. 30. Initially dried hydrogels were swelled in 5% ethanol aqueous solution containing polydatin at the concentration of 2 mM. Ethanol was used in order to provide the total solubility of polydatin in the

liquid phase. Uptake history data for the first stage were fitted to the power law $M(t)/M_\infty = kt^n$. Diffusion exponents close to $n = 0.56$ were obtained for both hydrogels, thus suggesting an anomalous (non-Fickian) transport mechanisms [9, 96–98]. Coupling of diffusion and relaxation phenomena are therefore intervenient in these hydrogel loading processes.

Loaded hydrogels were thereafter dried at 40 °C and submitted to a release process for polydatin in a 5% ethanol aqueous solution. Concentration of polydatin in the liquid phase was measured for different time instants using UV absorption. Figure 31 shows the analysis of experimental data up to 60% release fraction. A diffusion exponent close to $n = 1$ was estimated with HCEL-8, indicating a Case II transport drug release mechanism [9, 96–98] and very close to a zero-order device under these conditions (constant release rate). The diffusion exponent calculated for HCEL-5 was n~0.88; it is also compatible with an anomalous transport mechanism, coupling diffusion and relaxation, but with prevalence of the latter, as further discussed in the next section where the release of polydatin from hydrogels impregnated at supercritical conditions is analyzed.

9 Supercritical Fluid Technology Applications with Polymer Networks and Hydrogels

9.1 Overview

One of the largest potential applications of supercritical fluid technology is the area of polymer synthesis and polymer processing (see [103], Chap. 5, concerning the polymer-supercritical fluid calculations). Indeed, it is well known that supercritical fluids have properties between those of a gas and a liquid, allowing, e.g., to compromise between high diffusion rates and high solubility in many complex mixtures. Based on these and many other advantages (e.g.," green technology," low toxicity in food, pharmaceutical, biomedical applications, etc.), supercritical fluid technology has been used in many different areas, namely, the impregnation of polymers [104, 105], microencapsulation [106], hydrogels tailoring for different applications [107–110], and diverse ranges of polymer synthesis [103, 111–113] including also polymer networks and hydrogels (see [17] and references therein).

In any supercritical fluid technology application, knowledge on the thermodynamic parameters impacting the phase behavior of the mixtures, namely, their solubility levels, is of utmost importance to understand and design the desired extraction, impregnation, separation, or reaction processes. In this context, equations of state (EOS) are especially useful to perform pressure-volume-temperature (PVT) calculations for the pure components and multicomponent mixtures. Peng-Robinson cubic EOS Eq. (38) is often used within this purpose for small molecules:

$$P = \frac{RT}{v-b} - \frac{a(T)}{v(v+b)+b(v-b)} \tag{38}$$

Above, v represents the molar volume of the fluid and a and b model parameters. Combining rules should be used to define these parameters when mixtures are used [103]. However, when huge polymer molecules are involved, these kinds of EOS are no longer valid, and alternative models must be used. The Sanchez-Lacombe EOS is very popular for polymer-supercritical calculations, being represented by:

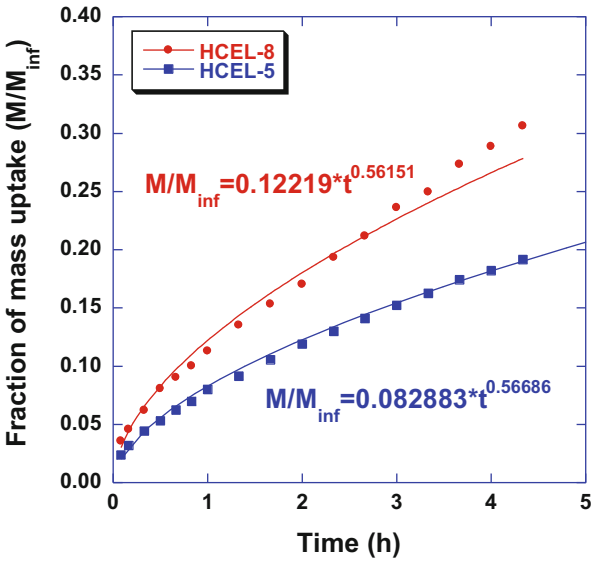

Fig. 30 Initial stage for the fraction of mass uptake, $M(t)/M_\infty$, during the swelling of two initially dried cellulose-based hydrogels in a 5% ethanol aqueous solution containing polydatin at a concentration of 2 mM. Dried hydrogels in the form of single cylinder pieces with typical diameter × thickness = 10 × 3 mm × mm were used. The equilibrium ("infinite") time was 6 days

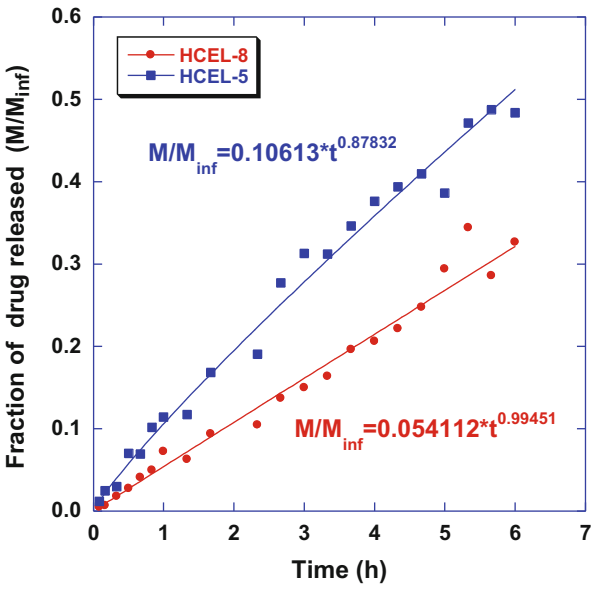

Fig. 31 Initial stage for the fraction of drug (polydatin) release, $M(t)/M_\infty$, from two initially dried cellulose-based hydrogels when poured into a 5% ethanol aqueous solution. The equilibrium ("infinite") release time was 6 days

$$\tilde{\rho}^2 + \tilde{P} + \tilde{T}\left[\ln(1-\tilde{\rho}) - \left(1 - \frac{1}{r}\right)\tilde{\rho}\right] = 0 \tag{39}$$

where $\tilde{P}$,$\tilde{T}$, and $\tilde{\rho} = 1/\tilde{v}$ represent the reduced pressure, temperature, and density, respectively. Definition of model parameters (r and other quantities) as well as combining rules for mixtures can be found elsewhere (see [103] and references therein).

9.2 A Case Study with the Impregnation of Polyphenols in Cellulose-Based Hydrogels

These tools are being used in our research to develop process conditions for different kinds of polymer synthesis and manipulation, namely, networks and hydrogels (e.g., molecular imprinting), cellulose-synthetic hybrids (RAFT-grafting, interpenetrating polymer networks), and materials impregnation for drug delivery. The upload of polydatin in cellulose-based hydrogels using supercritical CO_2 will be here considered to illustrate these kinds of applications.

Figure 32 shows an image of a cellulose hydrogel piece after impregnation with polydatin in supercritical CO_2 at T = 40 °C and P = 170 bar during 1 h. A 5% ethanol aqueous solution containing polydatin at the concentration of 2 mM was also included in the supercritical loading process. The speedup of the impregnation process with sc-CO_2 is one of the advantages introduced due to the higher diffusivity of the molecules in the network matrix, namely, the relatively high size polyphenol template used. Indeed, 1 hour was here used and around 6 days in the swelling process described in Sect. 8.

After impregnation with $ScCO_2$, hydrogels were dried at 40 °C in vacuum oven and submitted to a release process for polydatin in a 5% ethanol aqueous solution, as

Fig. 32 Image of a cellulose hydrogel piece after impregnation with polydatin in supercritical CO_2 at T = 40 °C and P = 170 bar during 1 h. A 5% ethanol aqueous solution containing polydatin at the concentration of 2 mM was also included in the supercritical loading process

before. Results for the dynamics of drug release are presented in Fig. 33, and, in spite of some scattering in the experimental data, steady state seems to be approached at around 60 h of release time.

Analysis of the period up to the first 60% drug release is performed in Fig. 34 where the fitting of the experimental data to the heuristic models $M(t)/M_\infty = kt^n$ and $M(t)/M_\infty = k_1 t^m + k_2 t^{2m}$ is also included. The latter model was developed to quantify

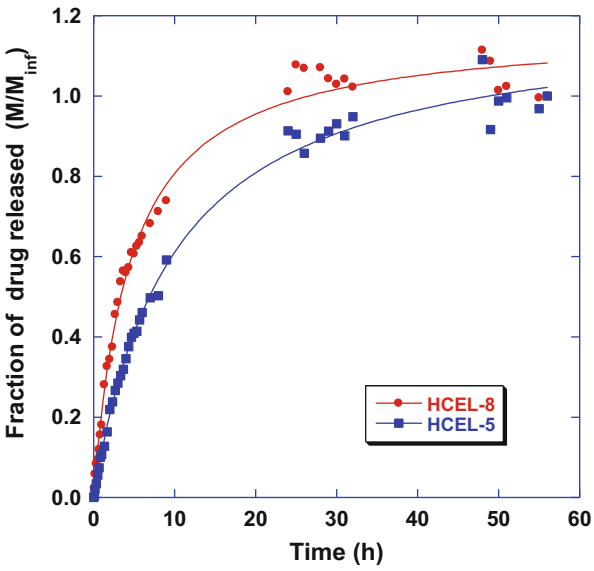

Fig. 33 Fraction of drug (polydatin) release, $M(t)/M_\infty$, from two initially dried cellulose-based hydrogels after pouring into a 5% ethanol aqueous solution. Impregnation of the polydatin in the hydrogels was previously performed in supercritical CO_2 at T = 40 °C and P = 170 bar during 1 h

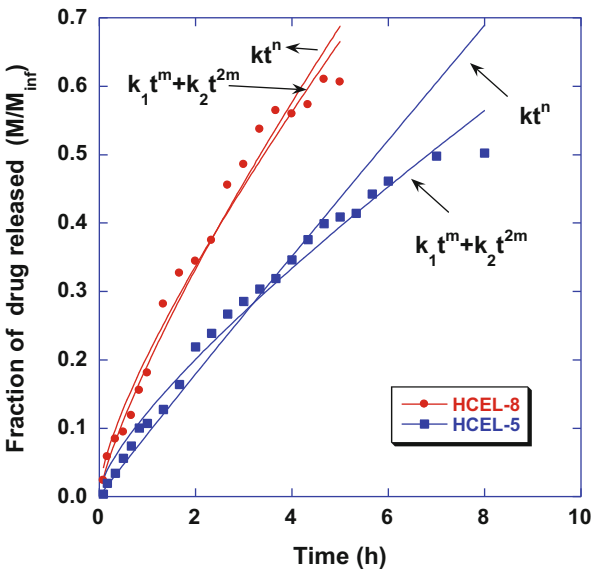

Fig. 34 Fraction of drug (polydatin) release, $M(t)/M_\infty$, from two initially dried cellulose-based hydrogels after pouring into a 5% ethanol aqueous solution. The period up to 60% drug release is here analyzed. Impregnation of the polydatin in the hydrogels was previously performed in supercritical CO_2 at T = 40 °C and P = 170 bar during 1 h

the relative contribution of the coupled diffusion and relaxation mechanisms, knowing the equation exponent (m) through the aspect ratio of the release device [98].

Considering the dimensions of the dried hydrogel pieces, the value $m = 0.43$ was used in our analysis [98]. With the base model, the diffusion exponents calculated for HCEL-8 and HCEL-5 are n~0.79 and n~0.97, respectively, putting into evidence again the anomalous transport mechanism involved. Discrimination of the diffusion and relaxation mechanisms can be estimated through the calculation of the parameters k_1 and k_2 in the second model. The following values were obtained: $k_1 = 0.078$ $h^{-0.43}$ and $k_2 = 0.128$ $h^{-0.86}$ with HCEL-8 and $k_1 = 0.048$ $h^{-0.43}$ and $k_2 = 0.075$ $h^{-0.86}$ with HCEL-5. Using these values, the Fickian release fraction [98] estimated for two cellulose-based hydrogels was obtained, and the results are presented in Fig. 35. After around 30 min release time, the polydatin liberation process starts to be clearly dominated by the relaxation of the polymer network for both hydrogels.

Results just presented show the usefulness of some simple tools to develop cellulose-based hydrogels (eventually including synthetic grafted chains) with tunable relaxation properties for drug release.

10 Conclusions

Polymer networks and hydrogels are "products-by-process" materials, and therefore their structure and final properties are defined during the synthesis process. Calculation tools with different degrees of complexity (and applicability), with the purpose of aiding the design of processes for the production of such materials, were presented

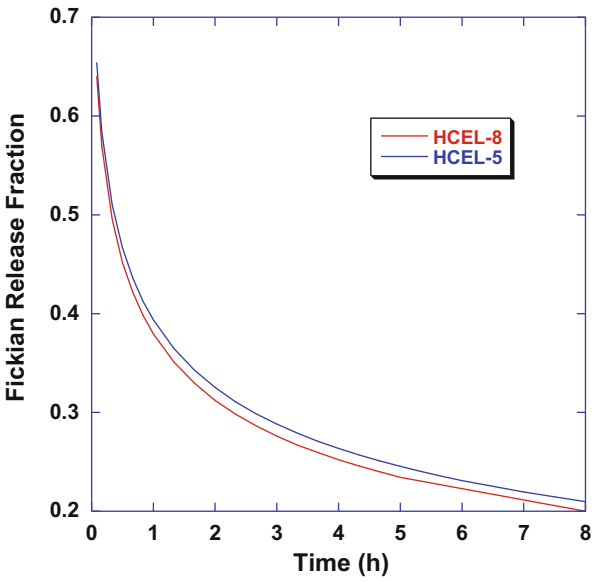

Fig. 35 Fickian release fraction estimated for two cellulose-based hydrogels considering the polydatin liberation in a 5% ethanol aqueous solution

and discussed. Some experimental tools to get information concerning the formation process and structure of polymer networks and hydrogels were also discussed (e.g., light scattering, swelling analysis, FTIR, SEC, etc.). Having in mind the importance of the generation of materials incorporating cellulose, the synthesis of cellulose-based hydrogels, the modification of the physicochemical properties of cellulose through cross-linking, and the RAFT-mediated grafting of synthetic polymers in cellulose were also here described. It was shown that the morphology and the molecular architecture of polymer networks and hydrogels can be changed using tools such as the reactor type (e.g., operation in batch or continuous flow micro-reactor), the polymerization process (e.g., considering bulk, inverse suspension, or precipitation polymerization), and the polymerization mechanism, namely, FRP or RDRP (RAFT polymerization was mainly addressed here). Different case studies were presented to illustrate the practical use of the produced materials in diverse applications, namely, MIP hydrogel particles to target aminopyridines, MIPs for polyphenols, caffeine or 5-fluorouracil, and also cellulose cross-linked with epichlorohydrin for polyphenol retention. The use of cellulose-based hydrogels as controlled release vehicles for polyphenols was also here addressed, and results for the liberation of these kinds of molecules were presented, evidencing the non-Fickian mechanisms involved in such transport systems. The possibility for the use of supercritical CO_2 in the hydrogel impregnation process was also shown.

11 Future Developments

Results here presented show that many different tools can be used to address the tailoring of polymer networks and hydrogels. However, the most promising techniques are based on the use of RDRP mechanisms due to the improved precision achieved in the molecular architecture of such materials. Moreover, with RDRP mechanisms, namely, the RAFT-mediated process, it is possible to improve the control of the grafting of synthetic polymers on the cellulose backbone. Many different engineered products with complex structures can therefore be designed, namely, molecularly imprinted polymers incorporating natural polymers such as cellulose.

Acknowledgments Parts of this work are a result of project "AIProcMat@N2020 – Advanced Industrial Processes and Materials for a Sustainable Northern Region of Portugal 2020," with the reference NORTE-01-0145-FEDER-000006, supported by Norte Portugal Regional Operational Programa (NORTE 2020), under the Portugal 2020 Partnership Agreement, through the European Regional Development Fund (ERDF) and of Project POCI-01-0145-FEDER-006984 – Associate Laboratory LSRE-LCM funded by ERDF through COMPETE2020 (Programa Operacional Competitividade e Internacionalização (POCI)) – and by national funds through FCT (Fundação para a Ciência e a Tecnologia). We also acknowledge the contribution of the master student Gayane Sadoyan in the framework of the thesis "Development of amphiphilic adsorbents for the stimulated uptake and release of polyphenols."

References

1. Galaev I, Mattiasson B (eds) (2008) Smart polymers. Applications in biotechnology and biomedicine. CRC Press, Boca Raton
2. Buchholz FL, Graham AT (1998) Modern superabsorbent polymer technology. Wiley-VCH, New York
3. Asúa JM (2007) Polymer reaction engineering. Blackwell Publishing, Oxford
4. Zohuriaan-Mehr MJ, Kabiri K (2008) Superabsorbent polymer materials: a review. Iran Polym J 17:451–477
5. Chang C, Zhang L (2011) Cellulose-based hydrogels: present status and application prospects. Carbohydr Polym 84:40–53
6. Kang H, Liu R, Huang Y (2016) Cellulose-based gels. Macromol Chem Phys 217:1322–1334
7. Chang C, Zhang L, Zhou J, Zhang L, Kennedy JF (2010) Structure and properties of hydrogels prepared from cellulose in NaOH/urea aqueous solutions. Carbohydr Polym 82:122–127
8. Zhou J, Chang C, Zhang R, Zhang L (2007) Hydrogels prepared from unsubstituted cellulose in NaOH/Urea aqueous solution. Macromol Biosci 7:804–809
9. Ciolacu D, Oprea AM, Anghel N, Cazacu G, Cazacu M (2012) New cellulose–lignin hydrogels and their application in controlled release of polyphenols. Mater Sci Eng C 32:452–463
10. Shibayama M (2017) Exploration of ideal polymer networks. Macromol Symp 372:7–13
11. Shibayama M (1998) Spatial inhomogeneity and dynamic fluctuations of polymer gels. Macromol Chem Phys 199:1–30
12. Kuru EA, Orakdogen N, Okay O (2007) Preparation of homogeneous polyacrylamide hydrogels by free-radical crosslinking copolymerization. Eur Polym J 43:2913–2921
13. Yazici I, Okay O (2005) Spatial inhomogeneity in poly(acrylic acid) hydrogels. Polymer 46:2595–2602
14. Flory PJ, Rehner J (1943) Statistical mechanics of cross-linked polymer networks. II. Swelling. J Chem Phys 11:521–526
15. Flory PJ (1950) Statistical mechanics of swelling of network structures. J Chem Phys 18:108–111
16. van Krevelen DW, Te Nijenhuis K (2008) Properties of polymers. Their correlation with chemical structure; their numerical estimation and prediction from additive group contributions, 4th edn. Elsevier, Amsterdam
17. Pérez-Salinas P, Jaramillo-Soto G, Rosas-Aburto A, Vázquez-Torres H, Bernad-Bernad MJ, Licea-Claverie Á, Vivaldo-Lima E (2017) Comparison of polymer networks synthesized by conventional free radical and RAFT copolymerization processes in supercritical carbon dioxide. Processes 5:1–23
18. Gonçalves MAD, Pinto VD, Dias RCS, Costa MRPFN (2010) FTIR-ATR monitoring and SEC/RI/MALLS characterization of ATRP synthesized hyperbranched polyacrylates. Macromol Symp 296:210–228
19. Gonçalves MAD, Pinto VD, Dias RCS, Costa MRPFN (2011) Kinetic modeling of the suspension copolymerization of styrene/divinylbenzene with gel formation. Macromol Symp 302:179–190
20. Gonçalves MAD, Pinto VD, Dias RCS, Costa MRPFN (2011) Modeling studies on the synthesis of superabsorbent hydrogels using population balance equations. Macromol Symp 306–307:107–125
21. Gonçalves MAD, Pinto VD, Costa RAS, Dias RCS, Hernándes-Ortiz JC, Costa MRPFN (2013) Stimuli-responsive hydrogels synthesis using free radical and RAFT polymerization. Macromol Symp 333:41–54
22. Gonçalves MAD, Pinto VD, Dias RCS, Costa MRPFN (2013) Polymer reaction engineering studies on smart hydrogels formation. JNPN 9/2:40–45

23. Gonçalves MAD, Pinto VD, Dias RCS, Hernándes-Ortiz JC, Costa MRPFN (2013) Dynamics of network formation in aqueous suspension RAFT styrene/divinylbenzene copolymerization. Macromol Symp 333:273–285
24. Aguiar LG, Gonçalves MAD, Pinto VD, Dias RCS, Costa MRPFN, Giudici R (2014) Mathematical modeling of NMRP of styrene divinylbenzene over the pre- and post-gelation periods including cyclization. Macromol React Eng 8:295–313
25. Oliveira D, Dias RCS, Costa MRPFN (2016) Modeling RAFT gelation and grafting of polymer brushes for the production of molecularly imprinted functional particles. Macromol Symp 370:52–65
26. Flory PJ (1941) Molecular size distributions in three dimensional polymers. I. Gelation. J Am Chem Soc 63:3083–3090
27. Flory PJ (1941) Molecular size distributions in three dimensional polymers. II. Trifunctional branching units. J Am Chem Soc 63:3091–3096
28. Flory PJ (1941) Molecular size distributions in three dimensional polymers. III. Tetrafunctional branching units. J Am Chem Soc 63:3096–3100
29. Flory PJ (1936) Molecular size distribution in linear condensation polymers. J Am Chem Soc 58:1877–1886
30. Flory PJ (1940) Molecular size distribution in ethylene-oxide polymers. J Am Chem Soc 62:1561–1562
31. Stockmayer WH (1943) Theory of molecular size distribution and gel formation in branched-chain polymers. J Chem Phys 11:45–55
32. Stockmayer WH, Jacobson H (1943) Gel formation in vinyl-divinyl copolymers. J Chem Phys 11:393–393
33. Stockmayer WH (1944) Theory of molecular size distribution and gel formation in branched polymers II. General crosslinking. J Chem Phys 12:125–131
34. Walling C (1945) Gel formation in addition polymerization. J Am Chem Soc 67(4):41–447
35. Walling C (1945) Correction. Gel formation in addition polymerization. J Am Chem Soc 67:2281–2281
36. Flory PJ (1953) Principles of polymer chemistry. Chapter 9. Cornell University Press, Ithaca
37. Good IJ (1962) Cascade theory and the molecular weight averages of the sol fraction. Proc Roy Soc A272:54–59
38. Gordon M, Scantlebury GR (1964) Non-random polycondensation: statistical theory of the substitution effect. Trans Faraday Soc 60:604–621
39. Macosko CW, Miller DR (1976) A new derivation of average molecular weights of non-linear polymers. Macromolecules 9:199–206
40. Beasley JK (1953) The molecular structure of polyethylene: IV. Kinetic calculations of the effect of branching on molecular weight distribution. J Am Chem Soc 75:6123–6127
41. Bamford CH, Tompa H (1954) The calculation of molecular weight distributions from kinetic schemes. Trans Faraday Soc 50:1097–1115
42. Zeman RJ, Amundson NR (1965) Continuous polymerization models – I. Polymerization in continuous stirred tank reactors. Chem Eng Sci 20:331–361
43. Zeman RJ, Amundson NR (1965) Continuous polymerization models – II. Batch reactor polymerization. Chem Eng Sci 20:637–664
44. Kuchanov SI, Pis'men LM (1971) The kinetic theory of gel formation in homogeneous radical polymerizations. Polym Sci USSR A13:2035–2048
45. Kuchanov SI, Pis'men LM (1972) Calculation of the polycondensation kinetics for monomers having reactive centres with different reactivities. Polym Sci USSR A14:147–160
46. Tobita H, Hamielec AE (1989) Modeling of network formation in free radical polymerization. Macromolecules 22:3098–3105
47. Teymour F, Campbell JD (1994) Analysis of the dynamics of gelation in polymerization reactors using the numerical fractionation technique. Macromolecules 27:2460–2469
48. Lazzari S, Storti G (2014) Modeling multiradicals in crosslinking MMA/EGDMA bulk copolymerization. Macromol Theory Simul 23:15–35

49. Bachmann R (2017) Extension of the method of moments in nonlinear free radical polymerization. Macromol Theory Simul 26:1–18
50. Costa MRPFN, Dias RCS (1994) A general kinetic analysis of non-linear irreversible copolymerisations. Chem Eng Sci 49:491–516
51. Costa MRPFN, Dias RCS (2005) An improved general kinetic analysis of non-linear irreversible polymerisations. Chem Eng Sci 60:423–446
52. Costa MRPFN, Dias RCS (2003) Prediction of sol fraction and average molecular weights after gelation for non-linear free radical polymerizations using a kinetic. Macromol Theory Simul 12:560–572
53. Dias RCS, Costa MRPFN (2003) A new look at kinetic modeling of nonlinear free radical polymerizations with terminal branching and chain transfer to polymer. Macromolecules 36:8853–8863
54. Dias RCS, Costa MRPFN (2005) Transient behavior and gelation of free radical polymerizations in continuous stirred tank reactors. Macromol Theory Simul 14:243–255
55. Dias RCS, Costa MRPFN (2005) Semibatch operation and primary cyclization effects in homogeneous free-radical crosslinking copolymerizations. Polymer 46:6163–6173
56. Dias RCS, Costa MRPFN (2006) A general kinetic method to predict sequence length distributions for non-linear irreversible multicomponent polymerizations. Polymer 47:6895–6913
57. Costa MRPFN, Dias RCS (2006) Kinetic modeling of non-linear polymerization. Macromol Symp 243:72–82
58. Costa MRPFN, Dias RCS (2007) Prediction of mean square radius of gyration of tree-like polymers by a general kinetic approach. Polymer 48:1785–1801
59. Dias RCS, Costa MRPFN (2007) Branching and crosslinking in coordination terpolymerizations. Macromol React Eng 1:440–467
60. Dias RCS, Costa MRPFN (2010) Calculation of CLD using population balance equations of generating functions: linear and non-linear ideal controlled radical polymerization. Macromol Theory Simul 19:323–341
61. Gonçalves MAD, Dias RCS, Costa MRPFN (2010) Modeling of hyperbranched polymer synthesis through atom-transfer and nitroxide-mediated radical polymerization of vinyl/divinyl monomers. Chem Eng Technol 33:1797–1813
62. Lazzari S, Hamzehlou S, Reyes Y, Leiza JR, Costa MRPFN, Dias RCS, Storti G (2014) Bulk crosslinking copolymerization: comparison of different modeling approaches. Macromol React Eng 8:678–695
63. Aguiar LG, Gonçalves MAD, Pinto VD, Dias RCS, Costa MRPFN, Giudici R (2014) Development of cyclic propagation kinetics for modeling the nitroxide-mediated radical copolymerization of styrene–divinylbenzene. Macromol React Eng 8:282–294
64. Dotson NA, Galván R, Laurence RL, Tirrel M (1996) Polymerization process modeling. Wiley-VCH, New York
65. Gonçalves MAD, Dias RCS, Costa MRPFN (2010) Prediction and experimental characterization of the molecular architecture of FRP and ATRP synthesized polyacrylate networks. Macromol Symp 289:1–17
66. Gonçalves MAD, Trigo IMR, Dias RCS, Costa MRPFN (2010) Kinetic modeling of the molecular architecture of cross-linked copolymers synthesized by controlled radical polymerization techniques. Macromol Symp 291–292:239–250
67. Espinosa-Perez L, Hernandez-Ortiz JC, Lopez-Domínguez P, Jaramillo-Soto G, Vivaldo-Lima E, Perez-Salinas P, Rosas-Aburto A, Licea-Claverie A, Vazquez-Torres H, Bernad-Bernad MJ (2014) Modeling of the production of hydrogels from hydroxyethyl methacrylate and (di) ethylene glycol dimethacrylate in the presence of RAFT agents. Macromol React Eng 8:564–579
68. Zapata-Gonzalez I, Saldívar-Guerra E, Ortiz-Cisneros J (2011) Full molecular weight distribution in RAFT polymerization. New mechanistic insight by direct integration of the equations. Macromol Theory Simul 20:370–388

69. Klumperman B (2015) Reversible deactivation radical polymerization. Enc Polym Sci Technol 1–27. https://doi.org/10.1002/0471440264.pst453.pub2
70. Matyjaszewski K, Spanswick J (2005) Controlled/living radical polymerization. Mater Today 8:26–33
71. Moad G, Rizzardo E, Thang SH (2012) Living radical polymerization by the RAFT process – a third update. Aust J Chem 65:985–1076
72. Moad G (2015) RAFT (Reversible addition fragmentation chain transfer) crosslinking (co) polymerization of multi-olefinic monomers to form polymer networks. Polym Int 64:15–24
73. Yan M, Huang Y, Lu M, Lin FY, Hernández NB, Cochran EW (2016) Gel point suppression in RAFT polymerization of pure acrylic cross-linker derived from soybean oil. Biomacromolecules 17:2701–2709
74. Kadhirvel P, Machado C, Freitas A, Oliveira T, Dias RCS, Costa MRPFN (2015) Molecular imprinting in hydrogels using reversible addition-fragmentation chain transfer polymerization and continuous flow micro-reactor. J Chem Technol Biotechnol 90:1552–1564
75. Pan G, Zhang Y, Guo X, Li C, Zhang H (2010) An efficient approach to obtaining water compatible and stimuli-responsive molecularly imprinted polymers by the facile surface-grafting of functional polymer brushes via RAFT polymerization. Biosens Bioelectron 26:976–982
76. Pan G, Ma Y, Zhang Y, Guo X, Li C, Zhang H (2011) Controlled synthesis of water-compatible molecularly imprinted polymer microspheres with ultrathin hydrophilic polymer shells via surface-initiated reversible addition-fragmentation chain transfer polymerization. Soft Matter 7:8428–8439
77. Ma Y, Zhang Y, Zhao M, Guo X, Zhang H (2012) Efficient synthesis of narrowly dispersed molecularly imprinted polymer microspheres with multiple stimuli-responsive template binding properties in aqueous media. Chem Commun 48:6217–6219
78. Zhang H (2013) Controlled/'living' radical precipitation polymerization: a versatile polymerization technique for advanced functional polymers. Eur Polym J 49:579–600
79. Zhao M, Chen X, Zhang H, Yan H, Zhang H (2014) Well-defined hydrophilic molecularly imprinted polymer microspheres for efficient molecular recognition in real biological samples by facile RAFT coupling chemistry. Biomacromolecules 15:1663–1675
80. Zhou T, Jørgensen L, Mattebjerg MA, Chronakis IS, Ye L (2014) Molecularly imprinted polymer beads for nicotine recognition prepared by RAFT precipitation polymerization: a step forward towards multi-functionalities. RSC Adv 4:30292–30299
81. Oliveira D, Gomes CP, Dias RCS, Costa MRPFN (2016) Molecular imprinting of 5-fluorouracil in particles with surface RAFT grafted functional brushes. React Funct Polym 107:35–45
82. Gurdag G, Sarmad S (2013) Cellulose graft copolymers: synthesis, properties, and applications. polysaccharide based graft copolymers. Chapter 2. In: Kalia S, Sabaa MW (eds) Polysaccharide based graft copolymers. Springer, Berlin/Heidelberg, pp 15–57
83. Kang H, Liu R, Huang Y (2015) Graft modification of cellulose: methods, properties and applications. Polymer 70:A1–A16
84. Anzlovar A, Huskic M, Zagar E (2016) Modification of nanocrystalline cellulose for application as a reinforcing nanofiller in PMMA composites. Cellulose 23:505–518
85. Barsbay M, Guven O, Davis TP, Barner-Kowollik C, Barner L (2009) RAFT-mediated polymerization and grafting of sodium 4-styrenesulfonate from cellulose initiated via γ-radiation. Polymer 50:973–982
86. Haqani M, Roghani-Mamaqani H, Salami-Kalajahi M (2017) Synthesis of dual-sensitive nanocrystalline cellulose-grafted block copolymers of N-isopropylacrylamide and acrylic acid by reversible addition-fragmentation chain transfer polymerization. Cellulose 24:2241–2254
87. Zeinali E, Haddadi-Asl V, Roghani-Mamaqani H (2014) Nanocrystalline cellulose grafted random copolymers of N-isopropylacrylamide and acrylic acid synthesized by RAFT

polymerization: effect of different acrylic acid contents on LCST behavior. RSC Adv 4:31428–31442
88. Moghaddam PN, Avval ME, Fareghi AR (2014) Modification of cellulose by graft polymerization for use in drug delivery systems. Colloid Polym Sci 292:77–84
89. Oliveira D, Freitas A, Kadhirvel P, Dias RCS, Costa MRPFN (2016) Development of high performance and facile to pack molecularly imprinted particles for aqueous applications. Biochem Eng J 111:87–99
90. Udoetok IA, Dimmick RM, Wilson LD, Headley JV (2016) Adsorption properties of cross-linked cellulose-epichlorohydrin polymers in aqueous solution. Carbohyr Polym 136:329–340
91. Domínguez-Avila JA, Wall-Medrano A, Velderrain-Rodríguez GR, Oliver Chen C-Y, Salazar-López J, Robles-Sánchez M, González-Aguilar GA (2017) Gastrointestinal interactions, absorption, splanchnic metabolism and pharmacokinetics of orally ingested phenolic compounds. Food Funct 8:15–38
92. Sellergren B (2001) Molecularly imprinted polymers man-made, mimics of antibodies and their applications in analytical chemistry. Elsevier, Amsterdam
93. Ye L, Mosbach K (2001) Molecularly imprinted microspheres as antibody binding mimics. React Funct Polym 48:149–157
94. Ye L, Mattiasson B (2015) Molecularly imprinted polymers in biotechnology. Springer International Publishing
95. Whitcombe MJ, Kirsch N, Nicholls IA (2014) Molecular imprinting science and technology: a survey of the literature for the years 2004–2011. J Mol Recognit 27:297–401
96. Ritger PL, Peppas NA (1987) A simple equation for description of solute release I. Fickian and non-Fickian release from non-swellable devices in the form of slabs, spheres, cylinders or discs. J Control Release 5:23–36
97. Ritger PL, Peppas NA (1987) A simple equation for description of solute release II. Fickian and anomalous release from swellable devices. J Control Release 5:37–42
98. Peppas NA, Sahlin JJ (1989) A simple equation for description of solute release III. Coupling of diffusion and relaxation. Int J Pharm 57:169–172
99. Peppas NA, Korsmeyer RW (1987) Dynamically swelling hydrogels in controlled release application. In: Peppas NA (ed) Hydrogels in medicine and pharmacy. CRC Press, Boca Raton
100. Kan W, Li X (2013) Mathematical modeling and sustained release property of a 5-fluorouracil imprinted vehicle. Eur Polym J 49:4167–4175
101. Crank J (1975) The mathematics of diffusion, 2nd edn. Oxford University Press, Oxford
102. Li H (2009) Smart hydrogel modeling. Springer, Berlin/Heidelberg
103. McHugh MA, Krukonis VJ (1994) Supercritical fluid extraction: principles and practice, 2nd edn. Butterworth-Heinemann, Newton
104. Kikic I, Vecchione F (2003) Supercritical impregnation of polymers. Curr Opin Solid State Mater Sci 7:399–405
105. Guney O, Akgerman A (2002) Synthesis of controlled-release products in supercritical medium. AICHE J 48:856–866
106. Sagis LMC (2015) Microencapsulation and microspheres for food applications. In: Sagis LMC (ed), Academic Press
107. Annabi N, Nichol JW, Zhong X, Chengdong J, Koshy S, Khademhosseini A, Dehghani F (2010) Controlling the porosity and microarchitecture of hydrogels for tissue engineering. Tissue Eng Part B 16:371–383
108. Tsioptsias C, Paraskevopoulos MK, Christofilos D, Andrieux P, Panayiotou C (2011) Polymeric hydrogels and supercritical fluids: the mechanism of hydrogel foaming. Polymer 52:2819–2826
109. Palocci C, Barbetta A, Grotta AL, Dentini M (2007) Porous biomaterials obtained using supercritical CO_2-water emulsions. Langmuir 23:8243–8251
110. Cardea S, Baldino L, De Marco I, Pisanti P, Reverchon E (2013) Supercritical gel drying of polymeric hydrogels for tissue engineering applications. Chem Eng Trans 32:1123–1128

111. Mueller PA, Storti G, Morbidelli M (2005) The reaction locus in supercritical carbon dioxide dispersion polymerization. The case of poly(methyl methacrylate). Chem Eng Sci 60:377–397
112. Mueller PA, Storti G, Morbidelli M (2005) Detailed modelling of MMA dispersion polymerization in supercritical carbon dioxide. Chem Eng Sci 60:1911–1925
113. Chatzidoukas C, Pladis P, Kiparissides C (2003) Mathematical modeling of dispersion polymerization of methyl methacrylate in supercritical carbon dioxide. Ind Eng Chem Res 42:743–751